



Contents lists available at ScienceDirect

## Journal of Molecular Spectroscopy

journal homepage: [www.elsevier.com/locate/jms](http://www.elsevier.com/locate/jms)

# Symmetry and Fourier analysis of the ab initio-determined torsional variation of structural and Hessian-related quantities for application to vibration–torsion–rotation interactions in CH<sub>3</sub>OH

Li-Hong Xu<sup>a,\*</sup>, J.T. Hougen<sup>b</sup>, J.M. Fisher<sup>a</sup>, R.M. Lees<sup>a</sup><sup>a</sup> Centre for Laser, Atomic, and Molecular Sciences (CLAMS), Department of Physics, University of New Brunswick, Saint John, NB, Canada E2L 4L5<sup>b</sup> Optical Technology Division, National Institute of Standards and Technology, Gaithersburg, MD 20899-8441, USA

## ARTICLE INFO

## Article history:

Received 6 November 2009

In revised form 3 January 2010

Available online 11 January 2010

## Keywords:

Internal rotation

Vibration–torsion interactions

Large-amplitude motion

Methanol

Torsional variation in structure

Forces

Vibrational displacements

Hessian

## ABSTRACT

The aim of the present paper is to investigate the use of quantum chemistry calculations to obtain the torsional dependence of various structural and vibrational-force-field-related quantities that could help in estimating the vibration–torsion–rotation interaction terms needed to treat perturbations observed in the spectra of methanol-like molecules. We begin by using the Gaussian suite of programs to determine the steepest-descent path from a stationary point at the top of the internal rotation potential barrier in methanol to the equilibrium structure at the bottom of the barrier. This procedure requires determining the gradient  $\nabla V$  of the potential (as calculated in mass-weighted Cartesian coordinates) along the internal rotation path. In addition, we use the Gaussian suite to calculate the Hessian  $\nabla^2 V$  along this path and to generate from these second derivatives the  $3N - 7$  small-amplitude vibrational frequencies and the  $3N$  Cartesian vibrational displacements for each of these vibrations. We then symmetrize the internal coordinates used in presenting the structures, gradients, Hessians and vibrational displacements along the path to take into account the periodic variation of the behavior of the three methyl hydrogen atoms H<sub>i</sub> as they pass in turn through the C<sub>s</sub>-plane of the HOC frame. The symmetrized linear combinations of the CH<sub>i</sub> stretches, of the OCH<sub>i</sub> bends, and of the HOCH<sub>i</sub> dihedral angles of the methyl group depend on the internal rotation angle  $\gamma$  and they are determined by considering coordinate transformations from the G<sub>6</sub> permutation-inversion group appropriate for internally rotating methanol. This symmetrization procedure permits us to explore the feasibility of expressing the structures, gradients, Hessians, and vibrational displacement vectors along the internal rotation path as short Fourier series in  $\gamma$ , which is one of the main goals of this paper. In summary, we find that the symmetrized structures, gradients, and Hessians, as well as nine of the 11 projected vibrational frequencies and the vibrational displacement vectors for the three vibrations occurring primarily in the HOC frame can be expressed by short Fourier series expansions to their precision in the Gaussian output, and that these series involve only  $\sin 3n\gamma$  or only  $\cos 3n\gamma$  terms, as required by G<sub>6</sub> symmetry considerations. A preliminary discussion is given of why short Fourier expansions fail for the projected frequencies of the two methyl asymmetric stretches, and for the vibrational displacement vectors of the methyl group vibrational modes. Looking more closely at the symmetrized and projected  $3N \times 3N$  Hessian, we find algebraically that only elements in the  $(3N - 7) \times (3N - 7)$  small-amplitude-vibrational block of the Hessian are useful for spectroscopic problems. Non-zero elements in the rest of the  $3N \times 3N$  symmetrized and projected Hessian cannot be converted into quantities needed for perturbation studies.

© 2010 Elsevier Inc. All rights reserved.

## 1. Introduction

This is the fourth paper in a series investigating the possibility of obtaining from ab initio studies vibration–torsion–rotation parameters of sufficient accuracy to be directly useable in high-

resolution spectroscopic studies of internal-rotor molecules. The underlying premises of the present work are as follows. We investigate specifically quantities appearing in the vibration–torsion–rotation Hamiltonian for the methanol molecule in its ground electronic state, as determined using quantum chemistry computational techniques. Methanol, however, can be considered as a prototype of the much broader class of molecules with  $3N - 7$  small-amplitude vibrations, one periodic large-amplitude motion, and C<sub>s</sub> point group symmetry in its equilibrium configuration.

\* Corresponding author. Fax: +1 506 648 5948.

E-mail address: [lxu@unb.ca](mailto:lxu@unb.ca) (L.-H. Xu).

Because of the periodicity of the large-amplitude motion, Fourier expansion techniques can be applied to almost all of the numerically computed structural and small-amplitude-vibrational results. Deviations from perfect periodic behavior tell us something about the accuracy of the calculations, and therefore something about how useful they will be in helping to guide high-resolution spectroscopic analyses. The number of terms in the Fourier expansions needed to fit the computational results tells us something about the rate of convergence of the model Hamiltonian commonly used. By concentrating on numerical variations of structural and vibrational parameters along the internal rotation path, we are implicitly hoping that such variations can be more accurately calculated than the absolute values of the corresponding parameters.

The first paper [1] in this series showed that quantum chemistry results for methanol at the top and bottom of the torsional barrier could be used to determine the torsional barrier height to better than 0.5%, and distortional contributions to differences of the rotational constants (three diagonal and one off-diagonal) at the top and bottom of the barrier (i.e., the first term in the Fourier expansion of their torsional variation) to accuracies ranging from 7% to 40%. Results for acetaldehyde were about 10 times worse, though these large discrepancies could be improved dramatically by empirically increasing at the barrier minimum and decreasing at the barrier maximum the angle between the  $\rho$  axis and the principal  $a$  axis by less than a degree. The second paper [2] described the torsional dependence of the  $\text{CH}_3$  stretching and bending modes of methanol in terms of a local mode internal coordinate picture [3]. The torsional variations of the small-amplitude vibrational frequencies along the mass-weighted intrinsic reaction coordinate from the top to the bottom of the torsional potential barrier were calculated by means of ab initio frequency projection utilizing GAUSSIAN 98 (G98) [4,5]. The resulting plots for the three C–H stretch ab initio frequencies as functions of the torsional angle were well-fitted when the  $3 \times 3$  local mode model [3] was extended to include higher-order coupling terms [2]. For the CH-bending modes, with internal coordinates chosen to give a high degree of localization, bend–torsion and bend–bend coupling parameters were determined from the ab initio projected frequencies, and were then used to predict torsional tunneling splittings. Just as observed for the C–H stretch modes, the two higher-frequency asymmetric methyl CH-bending modes were predicted to have inverted tunneling splittings with reduced amplitudes, while the splitting pattern for the lower frequency symmetric-bend mode was predicted to be normal. The third paper [6] showed that G98 delivered very smooth linear and quadratic force-constant plots as a function of angle along the internal rotation coordinate  $\gamma$  and that when coordinates symmetrized in the permutation inversion group  $G_6$  were used, each plot exhibited the  $\sin 3\gamma$  or  $\cos 3\gamma$  behavior expected from the symmetry species of the vibrational coordinate(s) that are multiplied by the given force constant. In spite of this excellent force-field behavior, however, the projected vibrational frequencies we obtained along the large-amplitude internal-rotation coordinate did not always extrapolate well to the vibrational frequencies obtained at the saddle and minimum of the potential surface (see Fig. 4 of [6]).

The aim of the present paper is to investigate the use of quantum chemistry calculations to obtain the torsional dependence of a variety of structural and vibrational-force-field-related quantities required for implementation of a vibration–torsion–rotation formalism proposed many years ago but not testable until the development of modern ab initio techniques. In this formalism [7,8], the large-amplitude internal rotation motion (LAM) is separated from the small-amplitude vibrations (SAV) and grouped with the rotational part of the Hamiltonian. The classical kinetic energy  $T$  can then be expressed in the form

$$2T = \boldsymbol{\omega} \cdot \mathbf{I} \cdot \boldsymbol{\omega} + (d\gamma/dt)^2 \left[ \sum_i m_i (d\mathbf{a}_i/d\gamma) \cdot (d\mathbf{a}_i/d\gamma) - 2 \sum_i m_i (d^2\mathbf{a}_i/d\gamma^2) \cdot \mathbf{d}_i \right] + 2(d\gamma/dt)\boldsymbol{\omega} \cdot \sum_i m_i (\mathbf{a}_i + 2\mathbf{d}_i) \times (d\mathbf{a}_i/d\gamma) + 2\boldsymbol{\omega} \cdot \sum_i m_i \mathbf{d}_i \times (d\mathbf{d}_i/dt) + \sum_i m_i (d\mathbf{d}_i/dt) \cdot (d\mathbf{d}_i/dt), \quad (1)$$

where  $\boldsymbol{\omega}$  is the four-dimensional angular velocity (containing the three Eulerian angle velocities and the LAM velocity  $d\gamma/dt$ ),  $\mathbf{I}$  is the corresponding  $4 \times 4$  moment of inertia,  $\mathbf{a}_i(\gamma)$  are the atom positions along the LAM path,  $\mathbf{d}_i$  are the infinitesimal SAV displacements from the  $\mathbf{a}_i(\gamma)$ ,  $m_i$  is the mass of atom  $i$ , and  $d/dt$  indicates a time derivative. The potential energy  $V$  takes one of two forms

$$V(\gamma, S) = V_o(\gamma) + \sum_i (\partial V/\partial S_i) S_i + (1/2) \sum_{ij} (\partial^2 V/\partial S_i \partial S_j) S_i S_j + \dots, \quad (2a)$$

$$V(\gamma, Q) = V_o(\gamma) + \sum_i (\partial V/\partial Q_i) Q_i + (1/2) \sum_i (\partial^2 V/\partial Q_i^2) Q_i^2 + \dots, \quad (2b)$$

where the form in Eq. (2a) is written in internal coordinates  $S_i$  for the 11 small-amplitude vibrations, and the form in Eq. (2b) is written in normal mode coordinates  $Q_i$  for these vibrations, so that  $(\partial^2 V/\partial Q_i^2)$  is a diagonal form of the Hessian containing the squares of the 11 projected vibrational frequencies.

To implement the treatment represented by Eqs. (1) and (2), one clearly requires functions of the internal rotation angle that describe atom positions, atom displacement vectors, and SAV forces and force-constants along the internal rotation motion. The present work explores the accuracy with which such functions can be obtained in convenient Fourier expansion form from current quantum chemistry capabilities.

In terms of Eq. (1), the present paper has the following parts. In Section 2 we return briefly to the question of defining the large-amplitude internal-rotation coordinate  $\gamma$ , and opt again for the steepest-descent definition of  $\gamma$ . In Section 3 we describe the origin of and solution to the numerical-discontinuity problems in our previous projected-frequency calculations [6] with G98. In Section 4 we consider the definition of a reference configuration  $\mathbf{a}_i(\gamma)$  in the molecule-fixed axis system along the large-amplitude coordinate  $\gamma$ , focusing in particular on the choice of orientation for this reference configuration in the molecule-fixed axis system. In Sections 5 and 6 we investigate whether useful information on the various derivatives with respect to  $\gamma$  in the Hamiltonian can be extracted directly from elements of the Hessian matrix along  $\gamma$  (i.e., from various second partial derivatives of the potential function at points along  $\gamma$ ). In Section 7 we present numerical ab initio results and Fourier expansion coefficients for the variation of the structure  $\mathbf{a}_i(\gamma)$ , Hessian  $H_{ij}(\gamma)$ , vibrational frequencies  $\nu_i(\gamma)$ , vibrational eigenvectors  $\mathbf{d}_i(\gamma)$ , and gradient  $\nabla V(\gamma)$  along the LAM coordinate  $\gamma$  in  $\text{CH}_3\text{OH}$ .

Section 8 contains a discussion and thoughts for future work. At the end of that discussion we consider very briefly one of the ways in which the present work is related to the much larger body of work on vibrational motions along a chemical reaction coordinate. In making such a comparison, the internal rotation motion must be thought of as an extremely rudimentary “reaction”, (i) whose initial state and final state are chemically indistinguishable (with identical energies, but with a different arrangement of previously numbered identical atoms), and (ii) whose reaction path (the internal rotation motion) involves no breaking of chemical bonds.

The extreme nature of these simplifications from chemical reactions as commonly understood, suggests that comparisons between these two related problems must be pursued with some care.

## 2. Definition of the large-amplitude coordinate

The choice of the large-amplitude coordinate and of the molecule-fixed axis system are both key questions when setting up a molecular Hamiltonian, since these choices influence the numerical values of any vibration–torsion–rotation interaction constants in the Hamiltonian which depend on derivatives of molecule-fixed components of force constants, atomic positions, and the like with respect to the large amplitude coordinate. For example, Refs. [9,10] discuss problems that arise in ab initio calculations when a large-amplitude internal-rotation coordinate is chosen which does not satisfy the usual threefold symmetry requirements. Ref. [6] discusses the sinusoidal relationship connecting any pair of internal-rotation coordinates that do satisfy the usual threefold symmetry requirements. Ref. [11] discusses subtle problems in the determination of the small-amplitude vibrational frequencies and coordinates, once a definition for the large-amplitude internal-rotation coordinate has been chosen.

We use here, as the primary definition of the large-amplitude internal rotation coordinate, the distance  $s$  along the path of steepest descent, in mass-weighted Cartesian coordinates, from the top of the barrier (saddle) to the bottom (potential minimum). (This distance can be converted to an angle with the desired threefold symmetry properties by the linear transformation in Eq. (2) of [6].) Distance along the path of steepest descent is often called the intrinsic reaction coordinate or IRC [12] and the steepest descent path from the saddle to the minimum is often called the minimum-energy path or MEP [13] in the chemical reaction-dynamics literature. Choosing the large-amplitude coordinate so it describes motion along the MEP has dynamical appeal, because a system point moving at infinitesimal velocity follows the MEP from the top of the potential barrier to the bottom. As mentioned in Ref. [11], the MEP has a number of disadvantages, e.g., it is not invariant to isotopic substitution and the distance  $s$  along the MEP is a non-local coordinate that can only be determined by solving a differential equation. In particular, the final value of  $s$  (at the bottom of the well) is often not well determined by the steepest-descent differential-equation algorithm and  $s$  is difficult to compare (both algebraically and numerically) between molecules.

We note in passing that non-mass-weighted Cartesian coordinates are most useful when discussing static (i.e., potential-energy) effects, since these depend only on interatomic distances. Mass-weighted coordinates become useful when kinetic-energy effects are considered, essentially because the kinetic energy  $(1/2)mv^2$  then becomes simply  $(1/2)v^2$ , or in the present context, because vibration frequencies squared are then directly proportional to eigenvalues of a Hessian matrix (i.e., a second derivative matrix) determined only from the potential energy function. In the equations and text of this paper we move back and forth between these two types of coordinates, depending on which is more convenient for the topic at hand.

Several papers (e.g., [9–11]) have advocated using the average of the three dihedral angles A–B–C–H<sub>i</sub> for the large-amplitude internal rotation coordinate, where C–H<sub>i</sub> with  $i = 4, 5, 6$  represents the methyl top and A and B are two atoms chosen from the frame. While such a coordinate is simple, has good symmetry properties, and is very close in value to the angular coordinate defined along the path of steepest descent for methanol and acetaldehyde (see Fig. 1 of [6] and Table 2 of [11]), the present authors prefer choosing the IRC as the formal theoretical definition of the large-amplitude coordinate because it avoids many of the complications

described in [11] for small-amplitude vibrational calculations along an LAM defined differently. It seems probable for many applications, however, that differences arising from these two large-amplitude coordinate definitions may be smaller than errors associated with the ab initio results. For this reason, and because of the problem of determining the final value of  $s$  mentioned above, we carry out Fourier expansions in later sections using an angle  $\gamma$  defined as the average of three dihedral angles A–B–C–H<sub>i</sub>, such that  $\gamma = 120^\circ$  at the top and  $\gamma = 180^\circ$  at the bottom of the barrier. This angle can be determined easily from standard Gaussian output. The distance  $s$  is retained as the large-amplitude coordinate in general discussions, however.

## 3. Projected-frequency calculations for the $1 \leq i \leq 3N - 7$ small-amplitude vibrations $\nu_i(s)$ from G03

It was pointed out in [6] that unexplained jumps of tens of  $\text{cm}^{-1}$  for acetaldehyde and a few  $\text{cm}^{-1}$  for methanol occurred at the first (saddle) and last (minimum) points of the projected frequency plots obtained directly from G98 [4]. Albu and Truhlar showed [14] that this problem could be eliminated by using the potential surface and first and second derivatives supplied by G98, but then using the GAUSSRATE [15] and POLYRATE [16] program suites to determine the MEP, molecular structures along the MEP, and projected frequencies for these structures. This led to the conclusion that the problem did not lie in the potential surface or potential-surface derivatives produced by Gaussian. As a further diagnostic, we found that applying the G98 projected frequency routine to the GAUSSRATE MEP structures gave results that agreed with Albu and Truhlar, strongly suggesting that the problem lay in G98's implementation of the steepest-descent algorithm and/or structural determinations along the steepest-descent path. The problem was first diagnosed precisely for us by Dr. Carlos Gonzalez at NIST, who pointed out [17] that the PATH command, which we had used in [6], determines the steepest descent path using redundant internal coordinates which are not mass-weighted [18]. A very thorough and very illuminating discussion of this question has been published recently by Allen et al. [11].

Briefly, the mathematical origins of our discontinuity problem can be summarized as follows. Consider a Taylor series expansion of an  $n$ -dimensional gradient vector about a stationary point  $\mathbf{X}_0 = \{x_i^0\}$ ,

$$\partial V / \partial x_i = [\partial V / \partial x_i]_{\mathbf{X}_0} + [\partial^2 V / \partial x_i \partial x_j]_{\mathbf{X}_0} dx_j + (1/2) [\partial^3 V / \partial x_i \partial x_j \partial x_k]_{\mathbf{X}_0} dx_j dx_k + \dots, \quad (3)$$

where the  $x_i$  represent mass-weighted coordinates and where the convention of summation over repeated indices is used. Confine attention to a region about the stationary point that is small enough to permit truncating the series for the gradient after the first non-vanishing term,

$$\partial V / \partial x_i \approx [\partial^2 V / \partial x_i \partial x_j]_{\mathbf{X}_0} dx_j \equiv \mathbf{H}_{ij} dx_j, \quad (4)$$

where the simplified notation  $\mathbf{H}$  is now used to represent the Hessian at the point  $\mathbf{X}_0$ . Then ask the general question of whether the gradient at an arbitrary point  $\mathbf{X}_1$  near the stationary point  $\mathbf{X}_0$  is parallel to the direction of the step from  $\mathbf{X}_0$  to  $\mathbf{X}_1$ , i.e., compute the scalar product  $p$  given by

$$p = dx_i (\partial V / \partial x_i) / |dx| |\partial V / \partial x| = dx_i \mathbf{H}_{ij} dx_j / |dx| [\mathbf{H}_{rs} dx_s \mathbf{H}_{rt} dx_t]^{1/2} \\ = dx_i \mathbf{H}_{ij} dx_j / |dx| [dx_s (\mathbf{H}^2)_{st} dx_t]^{1/2}, \quad (5)$$

where  $|dx|$  is the magnitude of the step vector, and compare the value of  $p$  to  $\pm 1$ . It is easy to show that if the step direction  $\mathbf{X}_1 - \mathbf{X}_0$  is parallel to an eigenvector of the Hessian matrix, i.e., if  $dx_i = \epsilon u_i$  where  $\epsilon$  is a smallness parameter and  $\mathbf{u}$  is a normalized eigenvector

satisfying  $\mathbf{H}\mathbf{u} = \lambda\mathbf{u}$ , then  $p = \lambda/|\lambda| = +1$  if the eigenvalue  $\lambda$  is positive (always the case at a local minimum), and  $p = -1$  when the eigenvalue  $\lambda$  is negative (as occurs for one eigenvalue at a first-order saddle point). It is also possible (though with somewhat more algebra) to show (if  $\mathbf{H}$  has no degenerate eigenvalues) that  $|p| < 1$  for all step directions not parallel to an eigenvector direction.

The final statements in the clarification of the projected-frequency discontinuity problem then become: (i) Calculating gradients away from the stationary points using non-mass-weighted coordinates will in general lead to gradients that are not parallel to the mass-weighted gradients. (ii) Projected-frequencies at points away from the stationary points will therefore be determined after projecting out the wrong coordinate direction, i.e., after projecting out some direction other than the mass-weighted steepest-descent direction. (iii) Projected vibrational frequencies along an ‘‘MEP’’ determined in this way will in general not extrapolate back to vibrational frequencies determined at the stationary points, since continuity at those points requires projecting out a direction after the first step from the saddle (or before the last step to the minimum) that is parallel to the eigenvector of the Hessian matrix in mass-weighted coordinates having a negative (or the smallest positive) eigenvalue.

As pointed out by Gonzalez [17], this problem can be fixed operationally in G03 by using the command **IRC**, because the default coordinates for **IRC** are mass-weighted internal (Z-matrix) coordinates. In fact, we used the **IRC** command in the G94 calculations reported in [1]. However, this requires using three separate jobs to map out the torsional potential, i.e., **OPT** for the local minimum, **QST3** for the first-order saddle point, and **IRC** for points in between, leading to a slight unsmoothness for structural and Hessian quantities near the top and bottom of the potential. The **PATH** command introduced in G98 gave much smoother structural and Hessian variation, since it allows for optimization of the top, bottom and points along the IRC in one job, but unfortunately, the **PATH** calculation does not follow a mass-weighted MEP. The best current option is thus to go back to the **IRC** command and three separate jobs, and to treat any unsmooth behavior along the MEP as the current level of ab initio noise. Ref. [11] explains how the problem can be fixed for other definitions of the large-amplitude internal-rotation coordinate.

#### 4. Orientation choices for reference configurations in the molecule-fixed axis system

Any attempt to define the reference configuration  $\mathbf{a}_i(s)$ , i.e., the set of molecular structures represented by the non-mass-weighted three-dimensional vector positions  $\mathbf{a}$  for each atom  $i$  at points along the large-amplitude coordinate  $s$ , raises two separate questions. The first concerns the molecular geometries themselves, and, as mentioned in Section 2, this is solved in a unique way by choosing to follow the steepest-descent path in mass-weighted Cartesian coordinates from the top of the barrier to the bottom. The second question concerns the orientation of the reference configuration in the molecule-fixed axis system at each point along the internal rotation coordinate. Internal-rotation Hamiltonians are often set up using one of three possible choices for the molecular orientation, namely the internal-axis-method (IAM), the principal-axis-method (PAM), or the rho-axis-method (RAM) Hamiltonians.

It turns out that structures obtained by solving the usual MEP differential equation [12] are automatically in an internal axis method (IAM) coordinate system [19], as shown by the following argument. The change in potential energy for an infinitesimal rotation of the molecule about any axis  $\mathbf{k}$  is zero, so that for any set  $\mathbf{r}$  of the  $N$  non-mass-weighted atomic Cartesian position vectors  $\mathbf{r}_i$ ,

$$\mathbf{0} = \sum_i \nabla_i V(\mathbf{r}) \cdot (\mathbf{k} \times \mathbf{r}_i) = \mathbf{k} \cdot \sum_i \mathbf{r}_i \times \nabla_i V(\mathbf{r}), \quad (6)$$

where  $\nabla_i$  is the gradient operator with respect to the non-mass-weighted Cartesian coordinates of atom  $i$ , and the second equality is a vector identity. Since  $\mathbf{k}$  could be chosen to be any of the unit vectors  $\mathbf{i}, \mathbf{j}, \mathbf{k}$  along the three Cartesian axes, Eq. (6) is equivalent to the vector equation

$$\mathbf{0} = \sum_i \mathbf{r}_i \times \nabla_i V(\mathbf{r}). \quad (7)$$

The differential equation defining molecular structures  $\mathbf{r}_i(s)$  along the MEP [12], can be written in non-mass-weighted coordinates as

$$m_i d\mathbf{r}_i/ds = -\nabla_i V/|\nabla_m V|, \quad (8)$$

where  $\nabla_m V$  represents the  $3N$ -dimensional potential gradient vector in mass-weighted Cartesian coordinates, i.e., a vector containing the quantities  $(m_i)^{-1/2} \nabla_i V$  for all  $N$  atoms, and  $|\nabla_m V|$  represents its magnitude. (N.B. Because non-mass-weighted coordinates are convenient for molecular structures and mass-weighted coordinates are convenient for the steepest descent gradient, there will be some alternation of usage in this paper. When both types of coordinates are used in the same numbered section, a difference in notation, e.g.,  $\nabla_i V$  and  $\nabla_m V$ , will be introduced.) At points  $\mathbf{r}_i(s)$  lying on the MEP one can now replace the gradient in Eq. (7) by an expression obtained from Eq. (8) to yield

$$\mathbf{0} = -|\nabla_m V| \sum_i \mathbf{r}_i(s) \times (m_i d\mathbf{r}_i/ds). \quad (9)$$

The non-mass-weighted reference-configuration coordinates  $\mathbf{a}_i(s)$  along the MEP will be in an IAM coordinate system [8,20] if no angular momentum is generated to first order by a change in the large-amplitude coordinate  $s$ , i.e., if

$$\mathbf{0} = \sum_i m_i \mathbf{a}_i(s) \times (d\mathbf{a}_i/ds). \quad (10)$$

It is clear from Eq. (9) that the molecular structures  $\mathbf{a}_i(s) \equiv \mathbf{r}_i(s)$  satisfy Eq. (10), i.e., the  $\mathbf{r}_i(s)$  obtained from Eq. (8) are all oriented in an IAM axis system.

At the top and bottom of the barrier  $\nabla_i V = \nabla_m V = \mathbf{0}$ , so that Eq. (8) is undefined. The direction of  $d\mathbf{r}_i/ds$  at the top of the barrier, where the steepest descent algorithm begins, is then defined to be the direction of the Hessian eigenvector with negative eigenvalue. At the bottom of the barrier one can show by mathematical arguments [21] that the MEP will ultimately enter the minimum of the well along the eigenvector direction with smallest eigenvalue. It can be shown, starting from Eq. (6), that Eq. (10) is satisfied at any point where  $\nabla_i V = \mathbf{0}$  and  $(d\mathbf{a}_i/ds)$  lies along the direction of an eigenvector of the Hessian belonging to a nonzero eigenvalue.

Unfortunately, G03 outputs structures along the steepest-descent path only after subjecting them to a subsequent rotation whose definition could not be located by the present authors, so that orientation information from the differential equation solution was not accessible. We have therefore chosen for most purposes to orient the structure given by G03 at each point along the MEP in its principal axis system, since this is simple to accomplish and easy to understand.

It is in principle possible to regenerate the IAM orientations corresponding to exact solutions of the steepest-descent differential equation in Eq. (8) using a procedure from the literature [22,23]. The steps would be the following (using notation and equation numbers from [23]). (i) Call the G03 structure at the saddle point in non-mass-weighted coordinates  $(\mathbf{a}_i)_{n=0}$ , and orient it in its principal axis system. (ii) Call the G03 structure at the first point along  $s$   $(\mathbf{a}_i)_{n=1}$ . (iii) In Eq. (4) of [23], identify  $(\mathbf{a}_i)_{n=0}$  with  $\mathbf{a}_i$  and  $(\mathbf{a}_i)_{n=1}$  with  $\mathbf{r}_i$ . (iv) Determine the rotational matrix  $Q$  from Eq. (6) of [23]. (v) Perform the rotation  $Q$   $(\mathbf{a}_i)_{n=1}$ . The structures  $(\mathbf{a}_i)_{n=0}$  and

$Q(\mathbf{a}_i)_{n=1}$  are now in orientations which satisfy Eqs. (8) and (10). (vi) Call the G03 structure at the second point after the saddle  $(\mathbf{a}_i)_{n=2}$  and use  $Q(\mathbf{a}_i)_{n=1}$  as the properly oriented structure for  $n = 1$ . Repeat steps (iii)–(v) with  $n \rightarrow n + 1$ . (vii) Continue iterating until the last G03 structure along  $\gamma$  has been processed. After that, all structures are in their correct orientation to satisfy Eqs. (8) and (10).

We note in passing, that a set of IAM orientations along an MEP is characterized only by the relative orientation between each member of the set. It is thus always possible to subject all members of an IAM set to the same arbitrary rotation without destroying their IAM character. Such an arbitrary rotation could be used, for example, to rotate any one member of the set into its principal axis system.

## 5. Linearly transformed versions of the Hessian matrix in the IAM coordinate system

The two lowest orders of force-field information are contained in the gradient  $\nabla_m V$  and Hessian  $\nabla_m \nabla_m V$  of the potential function  $V$ . At points on the MEP the first derivative of  $V$  with respect to mass-weighted coordinates  $(\nabla_m V)$  is tangent to the MEP, so the lowest-order force-field information for directions perpendicular to the MEP is contained in the second-derivative matrix, i.e., in the analog of the force-constant matrix at the potential minimum. During the course of this work, we derived algebraic expressions in terms of various derivatives of the potential energy function  $V$  for the information present at various locations in the  $3N \times 3N$  Hessian matrix, and found, contrary to our intuitive expectations, that terms in the off-diagonal blocks do not correspond directly to vibration–torsion–rotation coupling terms in the vibration–torsion–rotation Hamiltonian [7,8] shown in Eqs. (1) and (2). For this reason, we do not give these expressions here, but instead make only some general remarks.

One of the outputs of G03 at each point along the MEP is an accurate  $3N \times 3N$  Hessian matrix in non-mass-weighted Cartesian coordinates  $x_p$  (with  $p = 1, 2, \dots, 3N$ ) in the  $Z$ -matrix orientation, which contains second derivatives  $\partial^2 V / \partial x_p \partial x_r$  of the potential surface with respect to these non-mass-weighted coordinates. To gain physical insight into the molecular significance of the elements of this Hessian, it is convenient to linearly transform the Cartesian Hessian (i.e., to subject it to a similarity transformation at each point along the MEP) to a new set of coordinates  $q_j$  consisting of: (i)  $3N - 6$  coordinates specifying the instantaneous shape of the (nonlinear) molecule (where one of these can be the large-amplitude coordinate if desired); (ii) three rotational angles specifying the orientation of this molecular shape in space; and (iii) three translational coordinates specifying the position of the center of mass of this molecular shape in space. As recalled in Ref. [6], however, after linearly transforming to a set of  $3N - 6$  shape parameters consisting of both rectilinear and curvilinear coordinates (as will often be convenient when treating large-amplitude vibrational motions), many of the elements of the transformed Hessian matrix  $(\partial x_p / \partial q_j)(\partial^2 V / \partial x_p \partial x_r)(\partial x_r / \partial q_k)$  do not correspond to the true second derivatives  $\partial^2 V / \partial q_j \partial q_k$  of  $V$  with respect to  $q_j$  and  $q_k$ . Rearranging Eq. (14) of Ref. [6] yields

$$\sum_{p,r} (\partial x_p / \partial q_j) (\partial^2 V / \partial x_p \partial x_r) (\partial x_r / \partial q_k) = \partial^2 V / \partial q_j \partial q_k - \sum_p (\partial^2 x_p / \partial q_j \partial q_k) (\partial V / \partial x_p). \quad (11)$$

At the top (saddle) and bottom (minimum) of the MEP the gradient  $\nabla V = \mathbf{0}$ , so that the right-hand side of Eq. (11) reduces to a true second derivative of  $V$ . Algebraic expressions for the second term on the right of Eq. (11) can be obtained by differentiating twice an equation relating the laboratory-fixed non-mass-

weighted Cartesian coordinates  $\mathbf{R}_i$  of atom  $i$  (where  $i = 1, 2, \dots, N$ ) to the three laboratory-fixed Cartesian coordinates  $\mathbf{R}$  of the center of mass, the three rotational angles (Eulerian angles)  $\chi, \theta, \phi$ , the large-amplitude coordinate  $s$ , and the non-mass-weighted small-amplitude vibrational displacement vectors  $\mathbf{d}_i$  (depending linearly on  $3N - 7$  small amplitude vibrational coordinates  $Q_j$ , where  $j = 1, 2, \dots, 3N - 7$ ), i.e., by differentiating

$$\mathbf{R}_i = \mathbf{R} + S^{-1}(\chi\theta\phi)[\mathbf{a}_i(s) + \mathbf{d}_i(s, Q)], \quad (12)$$

Note that the  $x_p$  in Eq. (11) denote the non-mass-weighted laboratory-fixed Cartesian coordinates  $\mathbf{R}_i$  on the left of Eq. (12), and the  $q_j$  ( $i = 1, 2, \dots, 3N$ ) in Eq. (11) denote the set of  $3N$  “molecule-fixed” coordinates on the right of Eq. (12). For conceptual simplicity in the discussion below, we assume the  $3N$   $q$ ’s have been ordered as follows:  $q_j$  ( $j = 1, 2, \dots, 3N - 7$ ) =  $Q_j$  = the small-amplitude vibrations,  $q_{3N-6} = s$  = the large-amplitude motion,  $q_j$  ( $j = 3N - 5, 3N - 4, 3N - 3$ ) =  $\chi, \theta, \phi$  = the rotational angles, and  $q_j$  ( $j = 3N - 2, 3N - 1, 3N$ ) =  $R_x, R_y, R_z$  = the center-of-mass coordinates. Fig. 1 shows schematically a similarity-transformed Cartesian Hessian partitioned in this way. The results of rather lengthy algebraic operations (based on the ideas above) applied to elements lying in the 10 different blocks of the transformed Cartesian Hessian matrix partitioned as depicted in Fig. 1 can be summarized as follows. (We note in passing that the transformation matrix  $(\partial x_p / \partial q_j)$  in Eq. (11) is completely specified by taking: Cartesian displacements  $\Delta x_i, \Delta y_i, \Delta z_i$ , of the three translations of each atom  $i$  along the molecule-fixed  $\mathbf{i}, \mathbf{j}, \mathbf{k}$  axes, as usual; Cartesian displacements of the three rotations along  $\mathbf{i} \times \mathbf{a}_i, \mathbf{j} \times \mathbf{a}_i, \mathbf{k} \times \mathbf{a}_i$ , as usual; Cartesian displacements of the large-amplitude motion along the direction of steepest descent  $-\nabla_m V$ ; and Cartesian displacements of the  $3N - 7$  small-amplitude vibrations along vibrational displacement vectors satisfying the center-of-mass, Eckart, and Sayvetz conditions.)

### 5.1. Block B1

This block is obtained from Eq. (11) when both  $q_j$  and  $q_k$  are equal to small-amplitude vibrations, i.e., when  $q_j = Q_j$  and  $q_k = Q_k$ , for  $j, k = 1, 2, \dots, 3N - 7$ . Because the  $Q_j$  are defined to occur linearly in Eq. (12), all  $\partial^2 x_p / \partial Q_j \partial Q_k = 0$ , and elements in block B1 of the transformed Cartesian Hessian in Fig. 1 are thus all equal to true

	Q	$\gamma$	$\chi\theta\phi$	R
Q	B1			
$\gamma$		B3		
$\chi\theta\phi$		B5=0	B6	
R		B8=0	B9=0	B10=0

**Fig. 1.** Schematic diagram of the similarity-transformed  $3N \times 3N$  Hessian matrix on the left of Eq. (11) after partitioning into blocks labeled by the different types of molecule-fixed coordinates, namely: Q (the  $3N - 7$  small-amplitude vibrational coordinates);  $\gamma$  (the large-amplitude torsional coordinate);  $\chi, \theta, \phi$  (the three rotational coordinates (Eulerian angles)); and R (the three laboratory-fixed Cartesian coordinates of the center of mass). The 10 different kinds of blocks in this symmetric matrix are referred to by their numbers in the text.

second derivatives  $\partial^2 V / \partial Q_j \partial Q_k$  of the potential with respect to these rectilinear small-amplitude vibrational coordinates, i.e., elements in this block represent quadratic (harmonic) force constants, as they are commonly understood.

### 5.2. Blocks B7, B8, B9, and B10

These blocks are obtained from Eq. (11) when  $q_j$  and/or  $q_k \in \{\mathbf{R} = R_x, R_y, R_z\}$ . They can be shown to contain only zero elements to machine round-off precision, as might have been anticipated on physical grounds, since  $R$  represents the three translations of the molecule.

### 5.3. Blocks B4, B5, and B6

These blocks are obtained when  $q_j$  and/or  $q_k \in \{\chi, \theta, \phi\}$ . It turns out that only block B5 contains zeros to machine round-off precision (at points along the MEP and if  $\chi = \theta = \phi = 0$ ); blocks B4 and B6 contain non-zero combinations of products of quantities like  $(d\mathbf{a}_i^{\text{IAM}}/ds)$  and  $(\partial \mathbf{a}_i^{\text{IAM}} / \partial Q_k)$ . Close examination of these non-zero quantities shows, however, that they do not have the forms needed for Eq. (1).

### 5.4. Blocks B2 and B3

These blocks are obtained from Eq. (11) when  $q_j$  and/or  $q_k = s$ . They involve non-zero combinations of products of quantities like  $(d\mathbf{a}_i/ds)$ ,  $(\partial^2 \mathbf{d}_i / \partial s^2)$ , and  $(\partial^2 \mathbf{d}_i / \partial s \partial Q_k)$ , but again do not provide the expressions needed for Eq. (1).

Since none of the terms needed for the Hamiltonian appear in the off-diagonal blocks of the transformed Hessian shown in Fig. 1, it will be necessary to evaluate these Hamiltonian coefficients in a separate calculation involving various quantities and their first and second derivatives with respect to  $s$ . The Fourier expansions obtained in Section 7 should make such computations easier.

## 6. Transformed Hessian matrix in the PAM and RAM coordinate systems

The IAM results in Section 5 were all derived assuming that the vectors  $\mathbf{a}_i(s) + \mathbf{d}_i(s, Q)$  in Eq. (12) were expressed in an IAM coordinate system. However, this coordinate system is not often used in modern computations, so we reconsidered the results above for the PAM and RAM coordinate systems [19,20], which provide much simpler group theoretical considerations than the IAM system [20]. Conversion from the IAM system to the RAM or PAM systems can be represented formally by the equations

$$[\mathbf{a}_i(s) + \mathbf{d}_i(s, Q)]_{\text{RAM}} = M_{\text{RAM}}^{-1}(s)[\mathbf{a}_i(s) + \mathbf{d}_i(s, Q)]_{\text{IAM}}, \quad (13a)$$

$$[\mathbf{a}_i(s) + \mathbf{d}_i(s, Q)]_{\text{PAM}} = M_{\text{PAM}}^{-1}(s)[\mathbf{a}_i(s) + \mathbf{d}_i(s, Q)]_{\text{IAM}}. \quad (13b)$$

Conversion from the IAM system to the RAM system requires only a rotation  $M_{\text{RAM}}^{-1}(s)$  about the  $z$  axis, since the  $z$  axis is identical for those two systems. Conversion from IAM to PAM requires a full three-dimensional rotation matrix  $M_{\text{PAM}}^{-1}(s)$  since all three axes are changed.

It can be shown that some of the IAM results are unchanged by the use of RAM or PAM values for  $\mathbf{a}_i(s) + \mathbf{d}_i(s, Q)$ . In particular, the results for blocks B1 and B7–B10 above are unchanged, i.e., block B1 still contains the true second derivatives of the potential energy with respect to the small-amplitude vibrational coordinates and blocks B7–B10 still contain only zeros. However, the IAM results for blocks B2–B6 must be reexamined, since they all involve derivatives with respect to  $s$ , which will also act on the  $M^{-1}(s)$  matrices in Eq. (13), and/or involve the use of Eq. (8) to replace  $\partial V / \partial x_m$  by a

scalar times  $d\mathbf{a}_i^{\text{IAM}}/ds$ , which will not be possible for  $d\mathbf{a}_i^{\text{RAM}}/ds$  or  $d\mathbf{a}_i^{\text{PAM}}/ds$  since Eq. (8) is not valid for these quantities.

RAM and PAM results for blocks B2–B6 in Fig. 1 can be summarized by stating that all of these blocks are expected to contain non-zero elements, but none of these elements appears directly in the Hamiltonians of [7,8].

## 7. Symmetry properties and Fourier analysis of the ab initio results for methanol

In this section, we present our ab initio results for atom positions, Hessians, projected frequencies, vibrational eigenmode atomic displacement vectors, and the force vector along the steepest-descent gradient for methanol along the MEP. Since these five quantities represent the numerical results of ever increasing levels of mathematical manipulation of the potential surface (and therefore ever increasing levels of possible round-off errors), the question of numerical accuracy degradation of the ab initio results is of importance. We are particularly interested in whether or not these five quantities can be well represented by short Fourier expansions in the large-amplitude torsional coordinate  $\gamma$ , since the corresponding Fourier coefficients allow a compact representation of quantities computed at points along the MEP. This representation is convenient, because the various Fourier series can easily be differentiated algebraically to provide the derivatives with respect to  $\gamma$  required for setting up the final vibration–torsion–rotation Hamiltonian [8]. This representation is also informative, since the symmetry properties expected for the Fourier expansion of each quantity can serve as a check on the internal consistency of the numerical ab initio results.

The atom positions, Hessian matrix, projected frequencies, vibrational eigenvectors, and steepest-descent gradient presented here were all obtained from a two-step procedure with Gaussian 03 on the University of New Brunswick Chorus cluster, using the following commands. For the top of the barrier: (i) MP2 = Full/6-311+G(3df,2p) OPT = (Z-Mat,TS,NRSCALE,NOEIGEN,Vtight) NOSYMM, and (ii) MP2 = Full/6-311+G(3df,2p) NOSYMM FREQ = HPModes GEOM = Check. For the middle: (i) MP2 = Full/6-311+G(3df,2p) Geom = Check NOSYMM IRC = (Stepsize = 8,MaxPoints = 25,Forward,RCFC,VeryTight), and (ii) MP2 = Full/6-311+G(3df,2p) Freq = (Projected,HPModes), where the latter input structures along the MEP are from the IRC calculation outputs. For the bottom: (i) MP2 = Full/6-311+G(3df,2p) OPT = (Z-matrix,Vtight) NOSYMM, and (ii) MP2 = Full/6-311+G(3df,2p) NOSYMM FREQ = HPModes GEOM = Check. Even though points along the MEP were determined by following the path of steepest descent in mass-weighted coordinates, as explained in Section 2, we have used as our Fourier expansion variable the angle  $\gamma$ , i.e., the average of the three dihedral angles H–O–C–H<sub>i</sub>, where H<sub>i</sub> represents one of the three methyl hydrogens.

Computationally, we asked G03 to calculate 25 points with a stepsize of eight along the MEP, which translates to a total of 25 steps at 0.08 amu<sup>1/2</sup> Bohr per step [24]. This IRC stepsize led to an angular step size of approximately 3°, when internal rotation is measured by the average of the three dihedral angles, as shown in Table 1. In retrospect, our estimate of the IRC path length from top to bottom of the potential in amu<sup>1/2</sup> Bohr was too long. This, together with the fact that the IRC calculation tends to wander aimlessly at points very near the minimum, led us to exclude the last six data points from the IRC calculation. The remaining 19 IRC points were placed between the top (#1) and bottom (#21) points to form a nearly equally spaced IRC grid.

Most of the quantities desired here are given in the Gaussian output in more than one coordinate system and not necessarily in the same system from one quantity to another. This, and

**Table 1**

Values of the average dihedral angle  $\gamma^a$  along the steepest-descent path in mass-weighted coordinates for the 21 points<sup>b</sup> determined by G03.

Point <sup>b</sup>	Angle <sup>a</sup>
1	119.999494
2	122.87845
3	125.99511
4	129.11118
5	132.22655
6	135.34148
7	138.45549
8	141.56845
9	144.68024
10	147.79077
11	150.90000
12	154.00788
13	157.11441
14	160.21963
15	163.32361
16	166.42644
17	169.52827
18	172.62928
19	175.72968
20	178.82974
21	180.002052

<sup>a</sup> Average dihedral angle in degrees, keeping significant figures as given in the G03 output.

<sup>b</sup> Point number 1 is the saddle and point number 21 is the potential minimum. The extra digit emphasizes that these points were determined separately from the other 19 (see text).

symmetry requirements, necessitated numerous coordinate transformations which we now summarize. Gaussian uses three different Cartesian axis systems, called Z-matrix orientation, input orientation, and standard orientation. Molecular structures are provided as a set of three Cartesian coordinates in Å for each of the atoms, i.e., 18 numbers with six digits after the decimal, in each of these three systems. Molecular structures are also provided as a set of internal and redundant coordinates, with eight digits after the decimal. The precise form of these internal coordinates (bond lengths, bond angles, dihedral angles) is defined in the user-specified Z-matrix input file (not to be confused with the Cartesian Z-matrix orientation). We chose to use Cartesian-coordinate instead of internal-coordinate structures because the Hessian, of great interest for the present work, is outputted with more digits in its Cartesian-coordinate representation. In the present work, we first rotate the Cartesian coordinates of atoms in molecular structures along the MEP to bring each structure to a principal axis system that follows the usual spectroscopic convention for rotational constants, i.e.,  $A > B > C$ , as well as the commonly used  $I'$  representation relating  $a, b, c$  axis labels to  $x, y, z$  axis labels, i.e.,  $a = z, b = x, c = y$ . To permit symmetry analyses, we then define symmetry-adapted linear combinations of these principal-axis Cartesian atom coordinates, as discussed in connection with Eq. (15).

The  $3N \times 3N$  Hessian matrix, containing second derivatives of the potential function, can take a number of different forms, depending on whether derivatives are calculated with respect to mass-weighted or non-mass-weighted Cartesian coordinates or with respect to rectilinear or curvilinear internal coordinates. The Gaussian program provides Hessians in non-mass-weighted Cartesians (Z-matrix orientation, eight digits after the decimal) and rectilinear internal coordinates (bond lengths, bond angles, dihedral angles, five digits after the decimal). Since Cartesian Hessians are of better precision, we transformed each Cartesian Hessian along the MEP to its principal axis system, using the same  $3 \times 3$  rotation matrices as for the Cartesian structure principal-axis transformations. Since it is often useful to refer Hessian elements to internal coordinates resembling normal mode vibrations, we also performed a Cartesian to internal coordinate transformation using

Schachtschneider's GMAT program in its PC version [25], followed by a further internal coordinate symmetrization using Eqs. (16) and (17), with three translations and three rotations in the principal axis system [26] included and with proper mass weighting throughout. The  $3N \times 3N$  mass-weighted Hessian in the symmetrized internal coordinate system can then be considered to be partitioned into a  $(3N - 7) \times (3N - 7)$  block (B1 in Fig. 1), one LAM (12th row or column in Fig. 1), and three rotations and three translations (13th–18th rows or columns in Fig. 1).

The separation of the LAM from the rest was achieved via a Gram–Schmidt orthogonalization (Mathematica version), using as the unchanged (first) vector the normalized steepest descent vector (in symmetrized and mass-weighted internal coordinates) along the MEP. This vector can be obtained at all points along the MEP except the first and last (top and bottom of the potential curve) from the force vector provided by Gaussian (again, starting from the Cartesian representation because of its greater precision and then transforming to internal, and symmetrized internal coordinates with proper mass weighting). At the top and bottom of the potential curve the force is zero, so the MEP direction must be determined from the eigenvector with imaginary frequency at the top and with the smallest (torsional) frequency at the bottom. The ordering used in our Gram–Schmidt orthogonalization procedure was arbitrarily chosen as  $r_{\text{OH}}(A_1), r_{\text{CO}}(A_1), r_{\text{CH}}(S_1, A_1), r_{\text{CH}}(S_2, A_1), \beta_{\text{HOC}}(A_1), \beta_{\text{OCH}}(S_1, A_1), \beta_{\text{OCH}}(S_2, A_1), \tau_{\text{HOCH}}(S_3, A_1), r_{\text{CH}}(S_3, A_2), \beta_{\text{OCH}}(S_3, A_2), \tau_{\text{HOCH}}(S_2, A_2), 3\text{Ts}, 3\text{Rs}$ , where some of the 11 symmetrized internal coordinates are defined in terms of the linear combinations  $S_i$  in Eqs. (16) and (17). Note that the internal coordinate corresponding to the symmetrized “torsional” displacement vector  $\tau_{\text{HOCH}}(S_1, A_2)$ , which is in fact the average of the three HOCH dihedral angles, is not present in the list above. It will be replaced by the steepest descent vector (MEP direction), to which it is approximately equal, and any contribution of this steepest descent vector to the 11 internal coordinates in the list will then be removed by the Gram–Schmidt orthogonalization procedure.

Gaussian gives the projected vibrational eigenvectors at each MEP point in Cartesian displacements (standard orientation, five figures after the decimal). Unfortunately, the standard-orientation axis systems from point to point along the MEP can differ by two-fold rotations about any of the three Cartesian axes. Furthermore, the overall phase of the eigenvectors at each point can differ by  $-1$ . Thus, to smoothly connect the numerical entries given by Gaussian in an 18-dimensional Cartesian eigenvector at one point  $p$  along the MEP with its partner eigenvector at the next point  $p + 1$ , some appropriate combination of the rotations  $C_{2x}, C_{2y}, C_{2z}$  and the inversion  $i$  must be applied to the axis system at  $p + 1$ . Note that the appropriate combination of  $C_{2x}, C_{2y}, C_{2z}$  and  $i$  rotations for the  $(p, p + 1)$  pair can be different for different values of  $p$  along the MEP for eigenvectors corresponding to the same projected frequency, and can also be different for the same pair of MEP points (i.e., same  $p$  value) for eigenvectors corresponding to different projected frequencies, so that a total of  $11 \times 20 = 220$  (where 20 corresponds to the 20 IRC grid points after the first point at the top of the barrier) pairwise eigenvector “interfaces” must be carefully examined manually and corrected when necessary, before a mathematically meaningful variation of the vibrational eigenvector displacements with  $\gamma$  can be determined. The smoothly connected eigenvectors are then transformed to a principal axis system from their standard orientation.

To determine symmetry properties of various quantities taken from the G03 outputs, we use the procedures described in Ref. [20]. However, to make the atom numbering and internal rotation angle there agree with our present definitions and G03 outputs, it is necessary to make the following substitutions. In Fig. 1 and Table 8 of Ref. [20], remove the O atom in the aldehyde group, change  $C_a$  to  $O_2$ , and relabel  $H_a$  as  $H_1$ ; then relabel  $H_1, H_2, H_3$  in the methyl

group as  $H_4, H_6, H_5$ . In Eq. (7) and Table 8 of Ref. [20], replace  $\alpha$  by  $\pi - \gamma$ . These changes lead, for example, to symmetry transformations for the rotational ( $\chi, \theta, \phi$ ) and internal-rotational ( $\gamma$ ) variables in the present paper of the form:

$$(456)f(\chi, \theta, \phi; \gamma) = f(\chi, \theta, \phi; \gamma + 2\pi/3), \quad (14)$$

$$(56)^*f(\chi, \theta, \phi; \gamma) = f(\pi - \chi, \pi - \theta, \pi + \phi; -\gamma).$$

With this background, we now discuss Fourier series expansions of the numerical results and their related plots.

### 7.1. Molecular structure [3N = 18 functions = 6 vector functions $\mathbf{a}_i(\gamma)$ ]

Molecular structures are the first piece of information obtained from the ab initio calculations, in the sense that the relative positions of the  $N = 6$  atoms of methanol are used to specify the steepest descent path. These molecular structures are often given in terms of  $3N - 6$  bond lengths and bond angles, but for the purpose of constructing a vibration-torsion-rotation Hamiltonian [7,8], where Coriolis interactions take place along specific directions in the moment-of-inertia tensor, it is more useful to give atomic positions in a Cartesian axis system. In this work we have chosen to use the principal axis system for these atomic positions, because their variation with  $\gamma$  will then exhibit  $2\pi/3$  or  $2\pi$  periodicity, i.e., their Fourier coefficients must belong to definite symmetry species in  $G_6$ . (Fourier coefficients for atomic positions in the internal axis system belong to definite symmetry species only in the extended group  $G_6^{(m)}$  [20].)

Table 2 indicates that the variation with  $\gamma$  of atomic coordinates for the three frame atoms C–O–H in the principal axis system is well described by short Fourier expansions in  $\cos 3n\gamma$  ( $x$  and  $z$  components) or  $\sin 3n\gamma$  ( $y$  component). These forms for the expansions can be derived from symmetry considerations, as outlined above. Their simplicity arises essentially because frame atoms are not exchanged by any of the  $G_6$  PI operations. In Table 2 two sets of Fourier coefficients are given, one for expansions terminating at  $n = 2$ , the other for expansions terminating at  $n = 3$ . Since atom positions in Å are printed out by G03 to six decimal places, a perfect fit would lead to a root-mean-square deviation of  $2.9 \times 10^{-7}$ , a value obtained by assuming 10 equally probable errors of 0,  $\pm 1$ ,  $\pm 2$ ,  $\pm 3$ ,  $\pm 4$ ,  $5 \times 10^{-7}$  for a large set of numbers rounded to six decimal

places. This deviation of  $3 \times 10^{-7}$  is achieved for the  $n \leq 3$  fits and almost achieved for the  $n \leq 2$  fits of the O and C atom positions. The hydroxyl H atom positions, on the other hand, are fit five or 10 times worse. The question of optimal truncation (i.e., maximum  $n$ ) for the Fourier expansions is important when taking derivatives. It is well known that differentiating an infinite series reduces its convergence, an effect that is immediately obvious from the fact that  $d^2 \sin 3\gamma/d\gamma^2 = -9 \sin 3\gamma$ , while  $d^2 \sin 12\gamma/d\gamma^2 = -144 \sin 12\gamma$ . In any case, the full set of G03 frame-atom positions along the MEP, transformed to their principal axis systems, can be replaced with no loss in precision by the appropriate set of Fourier coefficients from Table 2.

Fourier expansions for the methyl hydrogen positions are more complicated. From a group theoretical point of view, this arises because these atoms are exchanged by operations of the PI group. From a physical point of view, this arises because these atoms pass in and out of the symmetry plane of the C–O–H frame during the internal rotation. It can be shown by using the symmetry procedures in [20], modified as described above, that the  $x$ - and  $z$ -coordinates of  $H_4$  and  $(1/2)(H_5 + H_6)$  and the  $y$ -coordinate of  $(1/2)(H_5 - H_6)$  can be fit to Fourier series in  $\cos n\gamma$ , while the  $y$ -coordinates of  $H_4$  and  $(1/2)(H_5 + H_6)$  and the  $x$ - and  $z$ -coordinates of  $(1/2)(H_5 - H_6)$  can be fit to Fourier series in  $\sin n\gamma$ . We have verified that Fourier expansions terminating at  $n = 6$  for these quantities in the PAM axis system along the 21 points of the MEP shown in Table 1 lead to standard deviations of  $3.5 \times 10^{-6}$  Å or less, but these fits are not presented in this work. Instead, we further symmetrize the methyl hydrogen coordinates to permit Fourier expansions in  $\cos 3n\gamma$  or  $\sin 3n\gamma$ . These symmetrized linear combinations have the form

$$\begin{aligned} \mathbf{S}_1 &= [\mathbf{a}_4(\gamma) + \mathbf{a}_5(\gamma) + \mathbf{a}_6(\gamma)]/3, \\ \mathbf{S}_2 &= [\cos \gamma \mathbf{a}_4(\gamma) + \cos(\gamma + 2\pi/3) \mathbf{a}_5(\gamma) + \cos(\gamma + 4\pi/3) \mathbf{a}_6(\gamma)]/3, \\ \mathbf{S}_3 &= [\sin \gamma \mathbf{a}_4(\gamma) + \sin(\gamma + 2\pi/3) \mathbf{a}_5(\gamma) + \sin(\gamma + 4\pi/3) \mathbf{a}_6(\gamma)]/3, \end{aligned} \quad (15)$$

where  $\Gamma(S_{1x}) = \Gamma(S_{1z}) = \Gamma(S_{2x}) = \Gamma(S_{2z}) = \Gamma(S_{3y}) = A_1$  in  $G_6$  and  $\Gamma$  for all other components is  $A_2$ . Table 3 indicates that the variation with  $\gamma$  of these more complicated linear combinations of atomic positions for the three methyl hydrogens in the principal axis system can be described to computational precision by short Fourier

**Table 2**

PAM positions in Å of the three frame atoms H, O, C for  $\text{CH}_3\text{OH}$  at the top ( $\gamma = 120^\circ$ ) and bottom ( $\gamma = 180^\circ$ ) of the barrier, and Fourier expansion coefficients in Å for these frame-atom positions along the MEP.

	x(H)	y(H)	z(H)	x(O)	y(O)	z(O)	x(C)	y(C)	z(C)
PAM positions of the H, O and C frame atoms in Å at the top and bottom of the barrier <sup>a</sup>									
Top	-0.819466	0.000000	1.049603	0.065268	0.000000	0.688759	-0.012450	0.000000	-0.727358
Bottom	-0.825629	0.000001	1.041489	0.063938	0.000000	0.687117	-0.013431	0.000000	-0.725461
Fourier expansion coefficients for $n \leq 2$ in Å for frame-atom positions along the MEP <sup>b</sup>									
$a_0$	-0.822529(1)	0 (fixed)	1.045559(2)	0.0646250(1)	0 (fixed)	0.6879669(4)	-0.0129330(2)	0 (fixed)	-0.7264409(3)
$a_3$	0.003086(1)	-0.006102(1)	0.004066(3)	0.0006640(2)	-0.0004022(3)	0.0008193(5)	0.0004896(2)	-0.0006974(1)	-0.0009469(4)
$a_6$	-0.000019(1)	0.000022(1)	-0.000013(3)	-0.0000221(2)	0.0000262(3)	-0.0000292(5)	-0.0000073(2)	0.0000083(1)	0.0000312(5)
$\sigma \times 10^{6c}$	3.8	3.4	8.7	0.7	0.9	1.7	0.8	0.5	1.5
Fourier expansion coefficients for $n \leq 3$ in Å for frame-atom positions along the MEP <sup>b</sup>									
$a_0$	-0.8225293(2)	0 (fixed)	1.0455587(3)	0.0646250(1)	0 (fixed)	0.6879669(1)	-0.0129330(1)	0 (fixed)	-0.7264409(1)
$a_3$	0.0030863(2)	-0.0061021(9)	0.0040680(5)	0.0006639(1)	-0.0004022(1)	0.0008190(1)	0.0004895(1)	-0.0006974(1)	-0.0009466(1)
$a_6$	-0.0000187(2)	0.0000223(9)	-0.0000135(5)	-0.0000220(1)	0.0000262(1)	-0.0000291(1)	-0.0000072(1)	0.0000083(1)	0.0000311(1)
$a_9$	-0.0000047(2)	0.0000024(9)	-0.0000109(5)	0.0000008(1)	-0.0000013(1)	0.0000021(1)	0.0000010(1)	-0.0000005(1)	-0.0000019(1)
$\sigma \times 10^{6c}$	0.8	3.0	1.6	0.3	0.2	0.3	0.3	0.3	0.3

<sup>a</sup> Cartesian structures in Z-matrix orientation at all points along the IRC, which are printed out with six decimal places by G03, have been rotated into their principal axis systems. Only structures at the top and bottom of the barrier are shown in this table. Since the molecule has an  $xz$ -plane of symmetry at the top and bottom of the barrier, the  $y$ -coordinates of all frame atoms are zero at these two points, but not at other points along the MEP.

<sup>b</sup> Fourier expansions for the  $x$ - and  $z$ -coordinates have the form  $\sum_n a_{3n} \cos 3n\gamma$ , where the maximum  $n$  is limited to either 2 or 3 in this table. Fourier expansions for the  $y$ -coordinates have the form  $\sum_n a_{3n} \sin 3n\gamma$ , where  $n = 0$  is not used in the sum. Numbers in parentheses indicate one standard uncertainty for the coefficients ( $k = 1$ , type A) [27], as given by the least-squares fits.

<sup>c</sup> The standard deviation  $\sigma$  in Å of each fit is given as  $\sigma \times 10^6$ .

**Table 3**  
Values in Å of symmetrized linear combinations<sup>a</sup> of PAM positions for the three methyl hydrogens in CH<sub>3</sub>OH at the top and bottom of the barrier, and Fourier expansion coefficients in Å for these linear combinations along the MEP.

	$x(S_1)$	$y(S_1)$	$z(S_1)$	$x(S_2)$	$y(S_2)$	$z(S_2)$	$x(S_3)$	$y(S_3)$	$z(S_3)$
Values in Å of symmetrized linear combinations of PAM positions of the three methyl H atoms at the top and bottom of the barrier <sup>a</sup>									
Top	-0.0227130	0.0000000	-1.1067257	-0.5087285	0.0000000	0.0119803	0.0000002	0.51100511	-0.0000001
Bottom	-0.0097337	-0.0000003	-1.1028610	-0.5080093	0.0000005	-0.0047300	0.0000009	0.5121700	-0.0000007
Fourier expansion coefficients in Å for $n \leq 3$ for the symmetrized linear combinations along the MEP <sup>b</sup>									
$a_0$	-0.0163748(1)	0 (fixed)	-1.1048279(1)	-0.5083694(1)	0 (fixed)	0.0038239(1)	0 (fixed)	0.5110913(1)	0 (fixed)
$a_3$	-0.0064832(1)	0.0069307(2)	-0.0019322(1)	-0.0003594(1)	-0.0023141(3)	0.0083465(2)	-0.0037281(3)	-0.0010594(1)	0.0090545(2)
$a_6$	0.0001507(1)	-0.0001784(2)	0.0000346(1)		-0.0000232(3)	-0.0001981(2)	-0.0000065(3)	0.0000191(1)	-0.0002320(2)
$a_9$	-0.0000064(1)	0.0000077(2)			0.0000031(3)	0.0000087(2)	0.0000032(3)		0.0000099(2)
$\sigma \times 10^{6c}$	0.5	0.5	0.3	0.3	0.8	0.6	1.1	0.3	0.5
Not fit <sup>d</sup>	-	-	-	-	pt. 20	-	pt. 20	-	pt. 20

<sup>a</sup> The linear combinations  $S_1$ ,  $S_2$  and  $S_3$  of the PAM methyl hydrogen positions used in this table are defined in Eq. (15). Only values at the top and bottom of the barrier are shown in this table.

<sup>b</sup> Fourier expansions for the  $x$  and  $z$  components of  $S_1$  and  $S_2$  and for the  $y$  component of  $S_3$  have the form  $\sum_n a_{3n} \cos 3n\gamma$ . Fourier expansions for the  $y$  component of  $S_1$  and  $S_2$  and for the  $x$  and  $z$  components of  $S_3$  have the form  $\sum_n a_{3n} \sin 3n\gamma$ , where  $n = 0$  is not used. Numbers in parentheses indicate one standard uncertainty ( $k = 1$ , type A) [27] for the Fourier coefficients, as given by the least-squares fits. Note that the maximum value of  $n$  used is different for different fits in this table, as indicated by various missing higher-order coefficients.

<sup>c</sup> The standard deviations  $\sigma$  of the fits are given as  $\sigma \times 10^6$ .

<sup>d</sup> When point number 20 is indicated in a given column, it was weighted zero in the fit because of its large obs. – calc. value.

expansions in either  $\cos 3n\gamma$  or  $\sin 3n\gamma$  which terminate at  $n = 3$  or less, i.e., Fourier expansions for these symmetrized combinations of methyl-hydrogen atom positions converge very much like the expansions for frame-atom positions.

## 7.2. Hessian matrix $[3N(3N + 1)]/2 = 171$ functions $H_{ij}(\gamma)$

In this section, we discuss elements  $H_{ij}(\gamma) = H_{ji}(\gamma)$  of the  $(3N - 7) \times (3N - 7)$  diagonal block of the Hessian obtained (starting from functions in the Cartesian system) when the three translations, three rotations, and large-amplitude motion are removed, and when derivatives are taken with respect to symmetry-adapted internal coordinates with proper mass weighting. We also discuss Fourier expansions of these elements in  $\sin 3n\gamma$  or  $\cos 3n\gamma$ , as required by symmetry considerations.

Symmetrized internal coordinates for the three vibrational motions not involving the methyl hydrogens are identical with the ordinary stretching coordinates  $r_{OH}$ ,  $r_{CO}$  and bending coordinate  $\beta_{HOC}$  in the frame, and are of species  $A_1$  in  $G_6$ . Symmetrized internal coordinates for the nine vibrational motions involving the methyl hydrogens can be obtained from equations analogous to Eq. (15), when the vectors  $\mathbf{a}_i$  are replaced by suitably defined scalars representing vibrational displacements  $\delta_i$  in the internal coordinates:

$$\begin{aligned} S_1 &= [\delta_4(\gamma) + \delta_5(\gamma) + \delta_6(\gamma)]/3, \\ S_2 &= [\cos \gamma \delta_4(\gamma) + \cos(\gamma + 2\pi/3) \delta_5(\gamma) + \cos(\gamma + 4\pi/3) \delta_6(\gamma)]/3, \\ S_3 &= [\sin \gamma \delta_4(\gamma) + \sin(\gamma + 2\pi/3) \delta_5(\gamma) + \sin(\gamma + 4\pi/3) \delta_6(\gamma)]/3. \end{aligned} \quad (16)$$

Three  $\delta_i$  ( $i = 4, 5, 6$ ) are defined for the C–H<sub>i</sub> stretches  $\delta r_i$ , three for the O–C–H<sub>i</sub> bends  $\delta \beta_i$ , and three for the H–O–C–H<sub>i</sub> dihedral angles  $\delta \tau_i$ , by the equations

$$\begin{aligned} \delta_i &= \delta r_i = \delta r(\text{C–H}_i), \\ \delta_i &= \delta \beta_i = \delta \beta(\text{O–C–H}_i), \\ \delta_i &= \delta \tau_i = \delta \tau(\text{H–O–C–H}_i). \end{aligned} \quad (17)$$

With these definitions,  $S_1(\delta r_i)$ ,  $S_1(\delta \beta_i)$ ,  $S_2(\delta r_i)$ ,  $S_2(\delta \beta_i)$ , and  $S_3(\delta \tau_i)$  are of species  $\Gamma = A_1$  in  $G_6$  (the same symmetry species as found for  $r_{OH}$ ,  $r_{CO}$  and  $\beta_{HOC}$  in the frame), the other four  $S_i$  are of species  $A_2$ . Since the potential energy function is  $A_1$ , and since the Hessian is the second derivative of the potential energy with respect to the various coordinates  $q_i$  above,  $\Gamma(H_{ij}) = \Gamma(q_i) \times \Gamma(q_j)$ . As mentioned earlier, to obtain a  $(3N - 7) \times (3N - 7)$  SAV diagonal block in the Hessian

matrix (block B1 in the  $3N \times 3N$  Hessian of Fig. 1) which corresponds to the force-constant matrix necessary for obtaining projected vibrational frequencies, the LAM (i.e., the  $\text{MEP} \approx S_1(\delta \tau_i)$  in Eq. (16)) is projected out using a Gram–Schmidt orthogonalization.

Fig. 2 of Ref. [6] illustrates the variation along the MEP of three elements of the “unprojected” Hessian matrix of methanol in symmetrized internal coordinates as given by Eqs. (16) and (17). The units of such matrix elements [4] are hartree/Bohr<sup>2-k</sup>rad<sup>k</sup>, where  $k = 0, 1$ , or 2 for stretch–stretch, stretch–angle, and angle–angle derivatives of the potential energy, respectively. (Note that the matrix product in the second line of the caption to Fig. 2 of Ref. [6] should be corrected to read  $S^t A^t F_{ij}(\gamma) B^{-1} S$ , to bring it into agreement with Eqs. (16) and (17) there.)

Fig. 2 here shows plots of a selection of 12 elements of the “projected” Hessian matrix. The label “projected Hessian matrix” is shorthand for the results of a multi-step procedure, involving several subtle details which can be explained (somewhat symbolically) as follows. (i) It is well known that eigenvalues  $\lambda_j$  of the  $GF$  matrix [28] in SI units are related to the vibrational frequencies in units of  $s^{-1}$  by  $\lambda_j = 4\pi^2 \nu_j^2$ . (ii) Consider two versions of the  $3N \times 3N$  matrices  $F$  and  $G$  along the MEP: a Cartesian version  $F_C$  and  $G_C$ , and an internal-coordinate version  $F_I = A^t F_C A$  and  $G_I = B G_C B^t$ , where the  $3N \times 3N$  matrices  $A$  and  $B$  have their usual meaning [26], as in Eq. (16) of Ref. [6]. (Since our  $G_C F_C$  matrix does not have SI units, but instead is in hartree/Bohr<sup>2</sup> u, where u is the <sup>12</sup>C atomic mass unit, some attention must be paid to conversion factors in the rest of this paragraph.) The  $B$  matrix used here was obtained from a program supplied by John Bertie [25]; rows corresponding to stretches were used as provided, but rows corresponding to angles were multiplied by the factor  $(1 \text{ \AA}) / (1.889 \text{ 276 Bohr})$ . (iii)  $G_C F_C$  is not Hermitian (not real symmetric in the present work), but  $G_C^{1/2} F_C G_C^{1/2}$  is, and  $|G_C^{1/2} F_C G_C^{1/2} - E \lambda| = 0$  gives the same secular equation as  $|G_C F_C - E \lambda| = 0$  [28]. We want to consider also the analogous product  $G_I^{1/2} F_I G_I^{1/2}$ , but a problem arises because  $G_I$  is not diagonal and its square root is not easily defined. This problem is overcome by first diagonalizing the real symmetric matrix  $G_I$  by a unitary (here real orthonormal) transformation  $U$ , then taking the square root, then transforming back to the “original” row and column labels with  $U^{-1}$ , i.e., by defining  $G_I^{1/2} = (B G_C B^t)^{1/2}$  to be  $U^{-1} [U (B G_C B^t) U^{-1}]^{1/2} U$ , where all matrices are  $3N \times 3N$ . (iv) We chose at this point to work with a  $GF$  matrix of the form  $S G_I^{1/2} F_I G_I^{1/2} S^t$ , where the  $3N \times 3N$  orthonormal matrix  $S$  forms

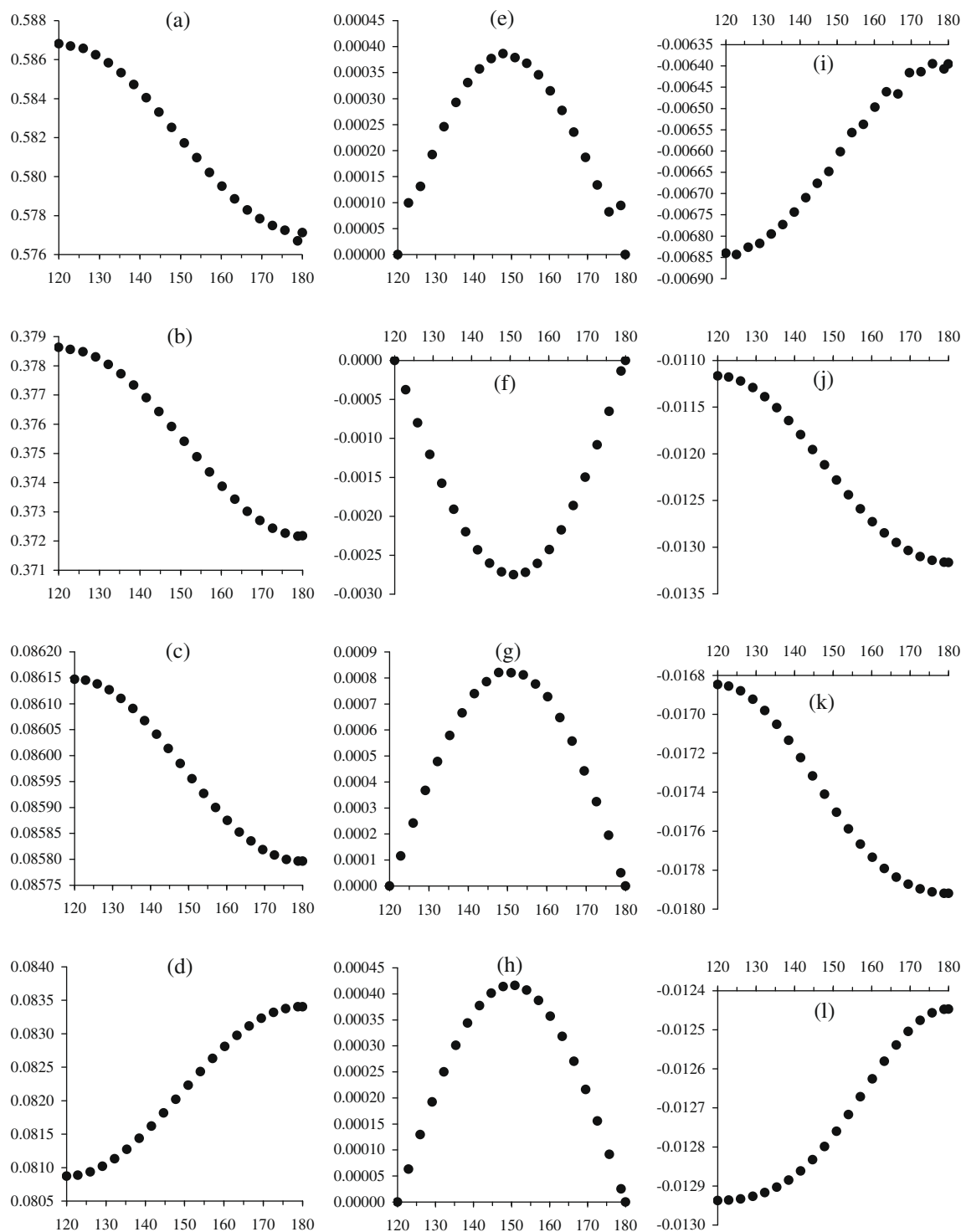


**Fig. 2.** Plots of 12 projected Hessian matrix elements as a function of the average dihedral angle  $\gamma$ , illustrating their cosine and sine variation. The abscissa for all panels is  $\gamma$ , and runs from 120° on the left (the top of the barrier) to 180° on the right (the potential minimum). The points are elements of the projected Hessian matrix  $PSG_1^{1/2}[A^T F_{ij}(\gamma)A]G_1^{1/2}S^{Pr}$  (see text), which was calculated starting from the  $3N \times 3N$  Cartesian force-constant matrix  $F_{ij}(\gamma)$  in our G03 output. Ordinate units are all hartree/Bohr<sup>2</sup> u. The bad points visible at position 20 in panels (a), (e), and (i) and elsewhere illustrate the limit of precision of these calculations. The four panels in the left column are all cosine curves, corresponding to diagonal elements of the projected Hessian for: (a) the OH stretch  $r_{OH}$  of species  $A_1$ , (b) a methyl CH stretch  $r_{CH}$  of species  $A_2$ , symmetrized as in  $S_3$  of Eq. (16), (c) a methyl OCH bend  $\beta_{OCH}$  of species  $A_1$ , symmetrized as in  $S_1$ , and (d) a vibration of species  $A_2$  involving the dihedral angles, symmetrized as in  $S_2$ . The four panels in the middle column are all sine curves, corresponding to off-diagonal elements of the projected Hessian involving one  $A_1$  vibration and one  $A_2$  vibration, i.e., panel (e) involves  $r_{OH}(A_1)$  and  $r_{CH}(S_3, A_2)$ , (f) involves  $r_{CH}(S_2, A_1)$  and  $r_{CH}(S_3, A_2)$ , (g) involves  $r_{CH}(S_3, A_2)$  and  $\beta_{OCH}(S_1, A_1)$ , and (h) involves  $\beta_{OCH}(S_1, A_1)$  and  $\tau(S_2, A_2)$ , where the shorthand notation for linear combinations and symmetry species associated with Eqs. (16) and (17) has been used. The four panels in the right column are again all cosine curves, corresponding to off-diagonal elements of the projected Hessian involving two  $A_1$  vibrations or two  $A_2$  vibrations, i.e., (i) involves  $r_{CO}(A_1)$  and  $r_{CH}(S_1, A_1)$ , (j) involves  $\beta_{HOC}(A_1)$  and  $\beta_{OCH}(S_2, A_1)$ , (k) involves  $r_{CH}(S_3, A_2)$  and  $\beta_{OCH}(S_3, A_2)$ , and (l) involves  $\beta_{OCH}(S_3, A_2)$  and  $\tau(S_2, A_2)$ . Fourier expansion coefficients for the cosine curves in the left column and for the sine curves in the middle column are given in the first and second rows of Table 4, respectively. Fourier expansion coefficients for the four cosine curves in the right column are not shown.

symmetrized linear combinations of the internal coordinates, as in Eqs. (16) and (17) here. We also work with a unit force vector obtained by normalizing  $SG_1^{1/2}f_i = SG_1^{1/2}A^{\text{tr}}f_c$ , where  $f_c$  is the  $3N \times 1$  vector containing the forces for Cartesian displacements of the atoms [4] along the MEP. (v) The next step is to project out the force direction from our internal coordinates by a Gram–Schmidt orthogonalization of a set of  $3N$  vectors. The first (unchanged) row contains the normalized  $SG_1^{1/2}A^{\text{tr}}f_c$  vector. Since the force along the MEP always points nearly along the internal rotation coordinate, this vector has a component of value near unity at the position of  $S_1(\tau, A_2)$  from Eq. (16), and components near zero elsewhere. The other row vectors in the pre-Gram–Schmidt procedure have exactly unity at one of the symmetrized internal coordinate positions and exact zeros elsewhere. (vi) The real orthonormal transformation matrix  $P$  obtained from the Gram–Schmidt procedure is then used to generate the “projected” Hessian matrix  $PSG_1^{1/2}F_iG_1^{1/2}S^{\text{tr}}P^{\text{tr}}$ . It is selected elements of this matrix that are illustrated in Fig. 2. Although a careful analysis of units is not presented here, all elements of the projected Hessian matrix are in hartree/Bohr<sup>2</sup> u, where u is the <sup>12</sup>C unit of mass.

Fig. 2(a)–(d) illustrates the cosine behavior of diagonal matrix elements of  $PSG_1^{1/2}F_iG_1^{1/2}S^{\text{tr}}P^{\text{tr}}$  for an  $A_1$  frame stretch ( $r_{\text{OH}}$ ), an  $A_2$  methyl-top stretch, an  $A_1$  methyl-top bend, and an  $A_2$  dihedral-angle linear combination. Fig. 2(e)–(h) illustrates the sine behavior of  $A_1/A_2$  cross terms for two stretch–stretch interactions, one stretch–bend interaction, and one bend–dihedral-angle interaction. Fig. 2(i)–(l) illustrates the cosine behavior of  $A_1/A_1$  or  $A_2/A_2$  cross terms for one stretch–stretch interaction, one bend–bend interaction, one stretch–bend interaction, and one bend–dihedral-angle interaction.

Table 4 represents eight of the curves in Fig. 2 by short Fourier cosine or sine expansions in the average torsional angle. Table 4 illustrates the fact that elements of the projected Hessian can be represented to about  $1 \times 10^{-5}$  hartree/Bohr<sup>2</sup> u by Fourier expansions in two or three-term  $\cos 3n\gamma$  or  $\sin 3n\gamma$  series.

A numerical consistency check on the procedures above is given by the fact that, as required by the algebraic considerations of Sections 5 and 6, the three rows and columns corresponding to translations in our projected Hessian matrix contain only entries smaller than  $10^{-9}$ . This, however, is five orders of magnitude larger than the double precision round-off error of  $10^{-14}$  or so expected

for a simple read-in/print-out cycle, but most of the additional error can be attributed to the precision of the structures (see Tables 2 and 3). These structures are required to carry out rotations to the principal axis system and to transform from Cartesian to internal coordinates, but they are given to only six decimal places in the G03 output.

### 7.3. Projected vibrational frequencies [ $3N - 7 = 11$ functions $v_j(\gamma)$ ]

As a check on our procedures and understanding up to this point we verified that the projected vibrational frequencies given in the G03 output could also be obtained by diagonalizing the  $(3N - 1) \times (3N - 1)$  block of the projected Hessian matrix obtained by discarding the first row and column. Six of the eigenvalues  $\lambda_j$  are nearly zero (corresponding to the three translations and three rotations deliberately kept in our diagonalization procedure as a check on the correctness and/or precision of our manipulations). The remaining  $3N - 7$  eigenvalues of the projected Hessian matrix were conveniently converted to vibrational frequencies  $v_j$  in  $\text{cm}^{-1}$  by using the expression  $v_j = \text{cnvt} * (\lambda_j)^{1/2}$ , where the factor  $\text{cnvt} = 5140.487$ . We have verified that projected frequencies obtained in this way agree with those given directly in the G03 output.

Physically, the 11 small-amplitude vibrational frequencies  $v_j(\gamma)$  in methanol must be invariant to the transformation  $\gamma \rightarrow \gamma + 2\pi/3$ , since this represents an exchange of identical particles, and to  $\gamma \rightarrow 2\pi - \gamma$ , since this represents reflection in the plane of symmetry at the  $\gamma = \pi$  equilibrium conformation. (Invariance under these two transformations can be used to derive invariance under  $\gamma \rightarrow \gamma + 2\pi$ , which represents the  $2\pi$  periodicity of the coordinate system, and  $\gamma \rightarrow 4\pi/3 - \gamma$ , which represents reflection in the plane of symmetry at the  $\gamma = 2\pi/3$  maximum of the barrier, so that the latter two transformations contain no new information.) These transformations (which follow the  $\gamma$  conventions of Table 1, corresponding to all our G03 outputs) can be used to show that the Fourier expansion of a projected frequency  $v_j(\gamma)$  should contain only terms of the form  $\cos 3n\gamma$ , where  $n$  is an integer.

Fig. 1 of Ref. [2] shows a plot of all 11 projected frequencies from an earlier calculation, exhibiting a maximum discontinuity of  $3 \text{ cm}^{-1}$  in the  $\nu_{11}(A_2)$  methyl out-of-plane rocking mode (see Section 3). Results from the present calculation would look similar

**Table 4**  
Fourier expansion coefficients for a few projected Hessian matrix elements<sup>a</sup>.

	$r_{\text{OH}}(A_1), r_{\text{OH}}(A_1)$ Cosine series <sup>b</sup>	$r_{\text{CH}}(S_3, A_2), r_{\text{CH}}(S_3, A_2)$ Cosine series <sup>b</sup>	$\beta_{\text{OCH}}(S_1, A_1), \beta_{\text{OCH}}(S_1, A_1)$ Cosine series <sup>b</sup>	$(\tau_{S_2}, A_2), \tau(S_2, A_2)$ Cosine series <sup>b</sup>
$a_0$	0.581967(2)	0.375478(2)	0.0859681(7)	0.0821540(5)
$a_3$	0.004839(3)	0.003223(3)	0.0001760(9)	−0.0012685(7)
$a_6$		−0.000083(3)		−0.0000157(7)
$\sigma \times 10^{5c}$	1.0	0.9	0.3	0.2
Not fit <sup>d</sup>	Pts. 2, 20	–	–	–
	$r_{\text{CH}}(S_3, A_2), r_{\text{OH}}(A_1)$ Sine series <sup>e</sup>	$r_{\text{CH}}(S_2, A_1), r_{\text{CH}}(S_3, A_2)$ Sine series <sup>e</sup>	$r_{\text{CH}}(S_3, A_2), \beta_{\text{OCH}}(S_1, A_1)$ Sine series <sup>e</sup>	$\beta_{\text{OCH}}(S_1, A_1), \tau(S_2, A_2)$ Sine series <sup>e</sup>
$a_0$	0 (fixed)	0 (fixed)	0 (fixed)	0 (fixed)
$a_3$	0.0003835(6)	−0.002749(1)	0.000826(1)	0.0004165(3)
$a_6$	0.0000165(6)	0.000071(1)	−0.000016(1)	
$\sigma \times 10^{5c}$	0.2	0.4	0.3	0.1
not fit <sup>d</sup>	pts. 2, 20	pts. 2, 20	–	–

<sup>a</sup> The eight projected Hessian elements in this table correspond to those shown in panels (a)–(h) of Fig. 2. The internal coordinates labeling the rows and columns of this Hessian have been symmetrized as in Eqs. (16) and (17) and orthogonalized by the Gram–Schmidt procedure. The  $a_0$  coefficient corresponds approximately to a normal projected Hessian element; the  $a_3$  and  $a_6$  coefficients describe the trigonometric variation of this element with internal rotation angle. All coefficients are in hartree/Bohr<sup>2</sup> u.

<sup>b</sup> Examples of cosine series expansions for diagonal projected Hessian matrix elements involving various stretching ( $r$ ), bending ( $\beta$ ), and dihedral ( $\tau$ ) coordinates.

<sup>c</sup> The standard deviation of the fit multiplied by  $10^5$ .

<sup>d</sup> Numbers shown in a given column of this row indicate points along the MEP that were removed from the fit of that column. Most of these bad points are clearly visible in the plots of these projected Hessian elements shown in Fig. 2.

<sup>e</sup> Examples of sine series expansions for off-diagonal projected Hessian matrix elements involving one coordinate of species  $A_1$  and one of species  $A_2$  in the permutation-inversion group  $G_6$ .

**Table 5**

Vibrational frequencies from G03 for CH<sub>3</sub>OH at the top and bottom of the barrier, Fourier expansion coefficients for the projected frequencies from G03 along the MEP, and G03-minus-Fourier-series values at the 21 points along the MEP.

	$\nu_1$	$\nu_2$	$\nu_9$	$\nu_3$	$\nu_4$	$\nu_{10}$
Vibrational frequencies $\nu$ in cm <sup>-1</sup> at the top (point 1) and bottom (point 21) of the barrier <sup>a</sup>						
$\nu_{\text{top}}$	3939.6368	3173.0735	3167.1614	3084.1029	1550.9880	1521.7472
$\nu_{\text{bottom}}$	3906.6430	3200.7185	3140.5033	3070.8489	1542.4691	1532.4390
Fourier expansion coefficients $a_{3n}$ in cm <sup>-1</sup> for the projected frequencies $\nu(\gamma)^b$						
$a_0$	3923.127(8)	3188.82(7)	3152.23(6)	3077.229(3)	1546.8451(6)	1527.276(2)
$a_3$	16.488(11)	-13.03(9)	12.54(9)	6.612(5)	4.2687(8)	-5.338(2)
$a_6$	-0.012(11)	-1.58(9)	1.21(9)	0.240(5)	-0.1188(8)	-0.174(2)
$a_9$		-0.60(9)	0.59(9)	0.017(5)	-0.0084(8)	-0.007(2)
$\sigma$	0.034	0.293	0.280	0.015	0.003	0.008
G03-minus-Fourier-series values in cm <sup>-1</sup> for projected frequencies at 21 points along the MEP						
1	0.03	-0.54	0.59	0.006	0.001	-0.009
2	-0.18 <sup>c</sup>	-0.36	0.23	-0.086 <sup>c</sup>	0.003	-0.006
3	0.03	0.15	-0.11	0.006	0.000	-0.003
4	-0.05	0.41	-0.41	-0.008	-0.001	0.007
5	-0.04	0.48	-0.44	-0.003	-0.002	0.008
6	-0.01	0.31	-0.31	-0.009	-0.003	0.012
7	0.00	0.10	-0.09	-0.005	-0.003	0.008
8	0.05	-0.11	0.12	0.001	-0.000	-0.001
9	0.03	-0.27	0.26	0.005	0.001	-0.006
10	-0.02	-0.30	0.26	-0.013	0.004	-0.009
11	-0.06	-0.22	0.21	0.012	0.001	-0.008
12	0.02	-0.04	0.08	0.012	0.000	-0.007
13	0.03	0.03	-0.06	0.006	0.001	-0.000
14	0.03	0.20	-0.19	-0.003	-0.000	0.004
15	-0.01	0.23	-0.19	0.014	-0.004	0.007
16	-0.04	0.16	-0.22	-0.050	0.001	0.013
17	-0.00	0.13	-0.07	0.007	-0.004	0.006
18	0.00	-0.01	0.02	0.002	0.000	0.002
19	-0.01	-0.20	0.12	-0.006	-0.001	-0.004
20	-1.47 <sup>c</sup>	-0.62 <sup>c</sup>	0.12 <sup>c</sup>	0.011	0.002	-0.006
21	0.02	-0.15	0.19	0.009	0.003	-0.008
Vibrational frequencies $\nu$ in cm <sup>-1</sup> at the top (point 1) and bottom (point 21) of the barrier <sup>a</sup>						
	$\nu_5$	$\nu_6$	$\nu_{11}$	$\nu_7$	$\nu_8$	$(\nu_2+\nu_9)/2$
$\nu_{\text{top}}$	1508.6810	1360.2481	1208.5064	1105.4699	1075.2683	3170.1175
$\nu_{\text{bottom}}$	1504.8854	1377.8753	1197.5911	1102.4868	1073.2326	3170.6109
Fourier expansion coefficients $a_{3n}$ in cm <sup>-1</sup> for the projected frequencies $\nu(\gamma)^b$						
$a_0$	1506.491(1)	1369.672(2)	1202.206(1)	1103.376(2)	1074.813(2)	3170.532(4)
$a_3$	1.883(2)	-8.790(2)	5.472(1)	1.519(2)	1.002(3)	-0.238(6)
$a_6$	0.288(2)	-0.609(2)	0.844(1)	0.605(2)	-0.566(3)	-0.180(6)
$a_9$	0.014(2)	-0.021(2)	-0.013(1)	-0.026(2)	0.019(3)	
$\sigma$	0.006	0.008	0.005	0.008	0.009	0.019
G03-minus-Fourier-series values in cm <sup>-1</sup> for projected frequencies at 21 points along the MEP						
1	0.006	-0.004	-0.002	-0.005	0.001	0.003
2	0.007	-0.008	0.002	-0.005	-0.003	-0.085 <sup>c</sup>
3	-0.000	-0.004	-0.002	-0.003	-0.000	0.001
4	-0.002	0.010	0.002	0.010	0.009	-0.015
5	-0.011	0.006	-0.002	0.000	-0.007	0.010
6	-0.005	0.010	0.003	0.012	0.007	-0.003
7	-0.005	0.004	0.000	0.003	-0.002	0.006
8	-0.002	-0.014	-0.000	-0.011	-0.016	0.007
9	0.005	-0.007	0.001	-0.001	-0.001	0.002
10	0.008	0.001	0.003	-0.003	0.003	-0.019
11	0.008	0.009	-0.003	0.006	0.018	-0.002
12	0.002	-0.004	-0.004	-0.003	0.005	0.017
13	0.000	-0.008	-0.002	-0.009	-0.009	-0.017
14	-0.004	-0.001	0.003	0.001	-0.004	0.005
15	-0.010	0.003	-0.006	-0.002	-0.007	0.019
16	0.001	0.014	0.013	0.013	0.007	-0.030
17	-0.006	-0.006	-0.002	0.004	-0.012	0.029
18	0.002	0.008	0.006	0.013	0.009	0.005
19	-0.001	-0.003	-0.007	-0.011	-0.003	-0.039
20	0.004	-0.008	-0.002	-0.009	-0.003	-0.248 <sup>c</sup>
21	0.004	0.001	-0.000	-0.001	0.007	0.021

<sup>a</sup> Points along the MEP are numbered from 1 (potential maximum) to 21 (potential minimum), and correspond to the  $\gamma$  values shown in Table 1. Vibrational numbering follows standard notation [29].

<sup>b</sup> Fourier expansions have the form  $\sum_n a_{3n} \cos 3n\gamma$ , where the maximum  $n$  is limited to either 2 or 3 in this table. Numbers in parentheses indicate one standard uncertainty ( $k = 1$ , type A) [27] from the least-squares fits.

<sup>c</sup> These points were weighted zero in the fits (see text).

on that scale, but with a maximum discontinuity of  $1.5 \text{ cm}^{-1}$  in the  $\nu_1(A_1)$  O–H stretching mode (see below), and are not re-plotted here. Table 5 shows the 11 small-amplitude vibrational frequencies from the present calculations at the maximum and minimum of the barrier, least-squares fitted coefficients of  $\cos 3n\gamma$  with  $n \leq 2$  or 3 for their Fourier expansions along the MEP, and G03 frequencies minus Fourier-series frequencies (i.e., obs. – calc. values) at the 21 points we calculated along the MEP.

All projected vibrational frequencies between  $1000 \text{ cm}^{-1}$  and  $1600 \text{ cm}^{-1}$  (i.e., all frequencies except the C–H and O–H stretches) can be fit to a four-term Fourier expansion to  $0.01 \text{ cm}^{-1}$  or better. Thus, this set of numerical projected frequencies from G03 can be replaced by their Fourier expansion coefficients with no loss in precision. Furthermore, these Fourier series are nicely convergent, with all  $a_9/a_6$  ratios smaller than 10.

The situation for the C–H and O–H stretches is different. After some preliminary fits, and as implied also by the bad points in a number of panels in Fig. 2, it became clear that frequencies at the first point after the maximum and at the last point before the minimum were often less well calculated than the rest. This is not surprising in retrospect, because the steepest-descent integration procedure makes use of the direction of the potential gradient at these points, and the very small absolute value of the gradient near the two stationary points may cause the numerical evaluation of its direction to suffer from round-off errors. In any case, one or both of these two points were weighted zero when calculating coefficients for the Fourier expansions for the hydrogen stretching vibrations. Once that is done,  $\nu_1$  (the O–H stretch) and  $\nu_3$  (the analog of the symmetric C–H stretch in  $\text{CH}_3\text{F}$ ) are relatively well behaved, though their standard deviations are from 5 to 10 times larger than for the lower frequency modes.

The Fourier expansions for  $\nu_2$  and  $\nu_9$  (corresponding to the two components of the degenerate C–H stretch in  $\text{CH}_3\text{F}$ ) are even less satisfactory, as shown in Table 5. A possible clue for this behavior is provided by recalling that diagonalization of a  $2 \times 2$  matrix puts square roots into the eigenvalue expressions, leading to a situation where convergence of the Fourier series for the resulting projected frequencies may be much slower than convergence of the Fourier series for the Hessian matrix elements themselves. It can further be seen from Table 5 that the Fourier coefficients and the residuals for  $\nu_2$  and  $\nu_9$  are nearly equal and opposite, which also strongly suggests trying to treat these two vibrations as an interacting pair, whose initial unperturbed frequencies  $\nu_2^0$ ,  $\nu_9^0$  and strength of inter-

action  $W$  might be well represented by short Fourier expansions. The formula for eigenvalues of a  $2 \times 2$  matrix then leads to considering an expression of the form

$$E_{\pm} = (1/2)(\nu_2^0 + \nu_9^0) \pm (1/2) \left[ (\nu_2^0 - \nu_9^0)^2 + 4W^2 \right]^{1/2}. \quad (18)$$

As shown in the last column of Table 5, the average  $(\nu_2 + \nu_9)/2$  can indeed be fit to  $0.02 \text{ cm}^{-1}$  by a three-term Fourier cosine series. (We note in passing that addition of a  $\cos 9\gamma$  term gives no improvement to the  $(\nu_2 + \nu_9)/2$  expansion.) Table 6 shows that

$$(\nu_2 - \nu_9)^2 = (E_+ - E_-)^2 = (\nu_2^0 - \nu_9^0)^2 + 4W^2 \quad (19)$$

can also be fit to a three-term Fourier cosine series with a standard deviation only slightly worse. (Again, addition of a  $\cos 9\gamma$  term gives no improvement.) The set of numerical values for  $(\nu_2 + \nu_9)/2$  and  $(\nu_2 - \nu_9)^2$  from G03 could thus, if desired, be replaced by their Fourier expansion coefficients in Tables 5 and 6 with essentially no loss in precision.

Since  $\nu_2$  is of species  $A'$  and  $\nu_9$  is of species  $A''$  when the molecule has  $C_s$  symmetry,  $W = 0$  at the top and bottom of the barrier, and its Fourier series should be a sine expansion. The  $2 \times 2$  model of an  $A_1$  vibration interacting with an  $A_2$  vibration via a sinusoidally varying interaction during the internal rotation process can then be pushed further by setting

$$\begin{aligned} \nu_2^0(\gamma) &= a_{2,0} + a_{2,3} \cos 3\gamma = 3186.89600 - 13.82250 \cos 3\gamma, \\ \nu_9^0(\gamma) &= a_{9,0} + a_{9,3} \cos 3\gamma = 3153.83235 + 13.32905 \cos 3\gamma, \end{aligned} \quad (20)$$

where values for the two coefficients in the Fourier expansions of Eq. (20) are obtained by fitting exactly to the values of  $\nu_2$  and  $\nu_9$  at the top and bottom of the barrier (see Table 5). The Fourier expansion of the interaction function  $W(\gamma)$  can then be obtained by setting

**Table 7**

Values for  $W$  in  $\text{cm}^{-1}$  from Eq. (21)<sup>a</sup> and G03-minus-Fourier-series values<sup>b,c</sup> in  $\text{cm}^{-1}$  from its Fourier expansion at 21 points<sup>d</sup> along the MEP.

Pt <sup>d</sup>	$W^a$	O–C <sup>b</sup>
1	0.00	0.00
2	1.59 <sup>c</sup>	0.05
3	3.13	–0.03
4	4.66	–0.04
5	6.10	–0.02
6	7.35	–0.02
7	8.42	–0.01
8	9.27	0.00
9	9.83	–0.02
10	10.18	0.00
11	10.23	–0.01
12	10.06	0.04
13	9.51	–0.03
14	8.89	0.07
15	7.85	–0.01
16	6.71	0.02
17	5.36	0.02
18	3.86	0.00
19	1.47 <sup>c</sup>	–0.80
20	0.00 <sup>c</sup>	–0.63
21	0.00	0.00

<sup>a</sup>  $W(\gamma) = (1/2) \{ [\nu_2(\gamma) - \nu_9(\gamma)]^2 - [\nu_2^0(\gamma) - \nu_9^0(\gamma)]^2 \}^{1/2}$ .  $W$  at point 20 was imaginary.

<sup>b</sup> G03-minus-Fourier-series =  $W(\gamma) - b_3 \sin 3\gamma$ , from the second equality in Eq. (21);  $b_3 = 10.246(9)$ , where one standard uncertainty from the least squares fit ( $k = 1$ , type A, Ref. [27]) is given in parentheses.

<sup>c</sup> Points were excluded from the fit, which gave a standard deviation  $\sigma = 0.03 \text{ cm}^{-1}$ .

<sup>d</sup> The average torsional angles corresponding to these 21 points are given in Table 1.

**Table 6**

Values for  $(\nu_2 - \nu_9)^2/100$  at the top (point 1) and bottom (point 21) of the barrier, Fourier expansion coefficients  $a_{3n}$  for  $(\nu_2 - \nu_9)^2/100$ , and G03-minus-Fourier-series values at the 21 points along the MEP, all in  $\text{cm}^{-2}$ .

Point	$(\nu_2 - \nu_9)^2/100^a$	$a_0$	$16.711(8)^b$
1	0.350	$a_3$	–17.953(11)
21	36.259	$a_6$	1.572(11)
		$\sigma$	0.033
G03-minus-Fourier-series values [ $\text{cm}^{-2}$ ] for $(\nu_2 - \nu_9)^2/100$ at 21 points along the MEP			
1	0.019	8	–0.002
2	0.025 <sup>c</sup>	9	–0.021
3	0.008	10	–0.007
4	–0.004	11	–0.015
5	–0.003	12	0.027
6	–0.009	13	–0.029
7	–0.007	14	0.053
		15	0.001
		16	0.023
		17	0.022
		18	0.019
		19	–0.098
		20	–0.454 <sup>c</sup>
		21	0.023

<sup>a</sup> Values of  $(\nu_2 - \nu_9)^2$  have been divided by 100 to make their total variation along the MEP, i.e., |(value at point 1) – (value at point 21)|, numerically comparable to the variations in Table 5.

<sup>b</sup> Fourier expansions have the form  $\sum_n a_{3n} \cos 3n\gamma$ , where  $n \leq 2$  in this table. Numbers in parentheses indicate one standard uncertainty ( $k = 1$ , type A) [27].

<sup>c</sup> These points were weighted zero in the fits.

$$W(\gamma) = (1/2) \left\{ [v_2(\gamma) - v_9(\gamma)]^2 - [v_2^0(\gamma) - v_9^0(\gamma)]^2 \right\}^{1/2} \\ = \sum_n b_{3n} \sin 3n\gamma. \quad (21)$$

Table 7 shows that a one term expansion in  $b_3 \sin 3\gamma$  with  $b_3 = 10.246(9) \text{ cm}^{-1}$ , represents the square root in Eq. (21) relatively well, since all residuals are less than  $0.08 \text{ cm}^{-1}$ , after removal of the first point after the saddle and the last two points before the minimum. Unfortunately, adding more sine terms does not decrease the residuals, indicating the quantitative limits of this simple  $2 \times 2$  model.

In summary, the very poorly convergent Fourier series for  $v_2(\gamma)$  and  $v_9(\gamma)$  in Table 5 can be replaced by a  $2 \times 2$  interaction matrix formulation, where Fourier series for the three independent elements of the  $2 \times 2$  matrix converge rather quickly. The deeper physical meaning of this empirical fact, as well as the connection of this  $2 \times 2$  formalism, with its  $\sin 3\gamma$  interaction term, to the  $3 \times 3$  formulation of Perry [3], with its  $\cos(\gamma)$  and  $\cos(\gamma \pm 2\pi/3)$  interaction terms, is not clear at present.

#### 7.4. Gradient vector [ $3N = 18$ functions] = $-\nabla V(\gamma)$

Gaussian provides the gradient vector expressed in both Cartesian components (18 components, Z-matrix orientation, nine digits after the decimal) and internal coordinate components (12 components, six digits after the decimal). As another test of Fourier series convergence properties, we show in Fig. 3 examples of six components of the normalized gradient vector in mass-weighted and symmetrized internal coordinates,  $SC_1^{1/2} A^{\text{tr}} f_C / |SC_1^{1/2} A^{\text{tr}} f_C|$ . The vector  $f_C$  was obtained originally from components of the direction of steepest descent, given by Gaussian in non-mass-weighted Cartesian coordinates in the Z-matrix orientation, but it was transformed into the PAM system before being used in the expression  $SC_1^{1/2} A^{\text{tr}} f_C$ . The symmetrization matrix  $S$  contains rows corresponding to  $S_1$ ,  $S_2$  and  $S_3$  in Eqs. (16) and (17) for the stretches  $\delta r(\text{C}-\text{H}_i)$ , bends  $\delta \beta(\text{O}-\text{C}-\text{H}_i)$ , and dihedral angles  $\delta \tau(\text{H}-\text{O}-\text{C}-\text{H}_i)$  of the methyl top. All elements of the gradient vector have units hartree/ $\text{u}^{1/2}$  Bohr. Fig. 3(a) shows the coefficient of the largest component of the gradient vector, which, apart from a small cosine dependence on  $\gamma$ , turns out as expected to be near unity and to lie along the torsional coordinate  $\tau_{\text{HOCH}}(S_1, A_2)$ . Fig. 3(b) and (c) gives the next two largest components, which are more than 10 times smaller and lie along the bending  $\beta_{\text{OCH}}(S_3, A_2)$  and rocking  $\beta_{\text{OCH}}(S_2, A_1)$  internal coordinates (see Tables 3 and 4 of Ref. [2] for the actual bending and rocking vibrational eigenmodes). Fig. 3(d)–(f) shows that components of the steepest-descent vector along the three stretching coordinates  $r_{\text{OH}}(A_1)$ ,  $r_{\text{CH}}(S_1, A_1)$  and  $r_{\text{CH}}(S_3, A_2)$ , which are expected by symmetry to be a sine, sine, and cosine curve, respectively, are at the noise level of the present quantum chemistry calculations.

There are two subtle points associated with the normalized gradient vector plots in Fig. 3. The first concerns symmetry properties. Because  $V(\gamma)$  is of species  $A_1$ , the species of  $\partial V/\partial q_i$  is the same as the species of  $q_i$  itself. The species of  $|\nabla V|$  is also  $A_1$ , so that the species of  $\partial V/\partial q_i / |\nabla V|$  is the same as the species of  $q_i$ . However, (without going into full detail), we note that  $|\nabla V|$  for our potential surface has a discontinuous first derivative at points where  $|\nabla V| = 0$  (just as  $|\gamma|$  has a discontinuous first derivative at  $\gamma = 0$ ). It turns out that this discontinuity and a number of unpleasant problems associated with it, in particular the slow convergence of Fourier expansions in its vicinity, can be removed if we consider normalized gradient vector elements of the form  $(\partial V/\partial q_i)(\sin 3\gamma) / |\nabla V| \cdot |\sin 3\gamma|$ , where  $(\sin 3\gamma) / |\sin 3\gamma| = \pm 1$  is just a variable phase factor that changes sign whenever  $|\nabla V| = 0$ . Since, however,  $(\sin 3\gamma) / |\sin 3\gamma|$  is of species  $A_2$  in  $G_6$ , the species  $\Gamma$  of normalized gradient vector elements of the form  $(\partial V/\partial q_i)(\sin 3\gamma) / |\nabla V| \cdot |\sin 3\gamma|$  are  $A_2 \times \Gamma(q_i)$ , i.e., the symmetry species of the curves in Fig. 3 are just the opposite of what one at first expects.

The second subtle point associated with elements of the normalized gradient shown in Fig. 3 concerns the points at the top and bottom of the barrier, where the gradient is zero. The normalized gradient then takes the form 0/0 and is therefore indeterminate. As discussed in Section 3, the steepest-descent gradient vector determined in mass-weighted Cartesian coordinates (which we use here) connects smoothly at the top of the barrier to the Hessian eigenvector with negative eigenvalue  $\lambda$  (and imaginary frequency  $\propto \lambda^{1/2}$ ), and connects smoothly at the bottom of the barrier to the Hessian eigenvector with smallest eigenvalue. We have therefore used these two eigenvectors in place of the indeterminate quantities  $\nabla V/|\nabla V|$  at the saddle point and at the minimum of the barrier.

#### 7.5. Vibrational displacements [ $(3N - 7) \times 3N = 11$ small-amplitude vibrations] $\times 18$ components $d_i(\gamma) = 198$ functions]

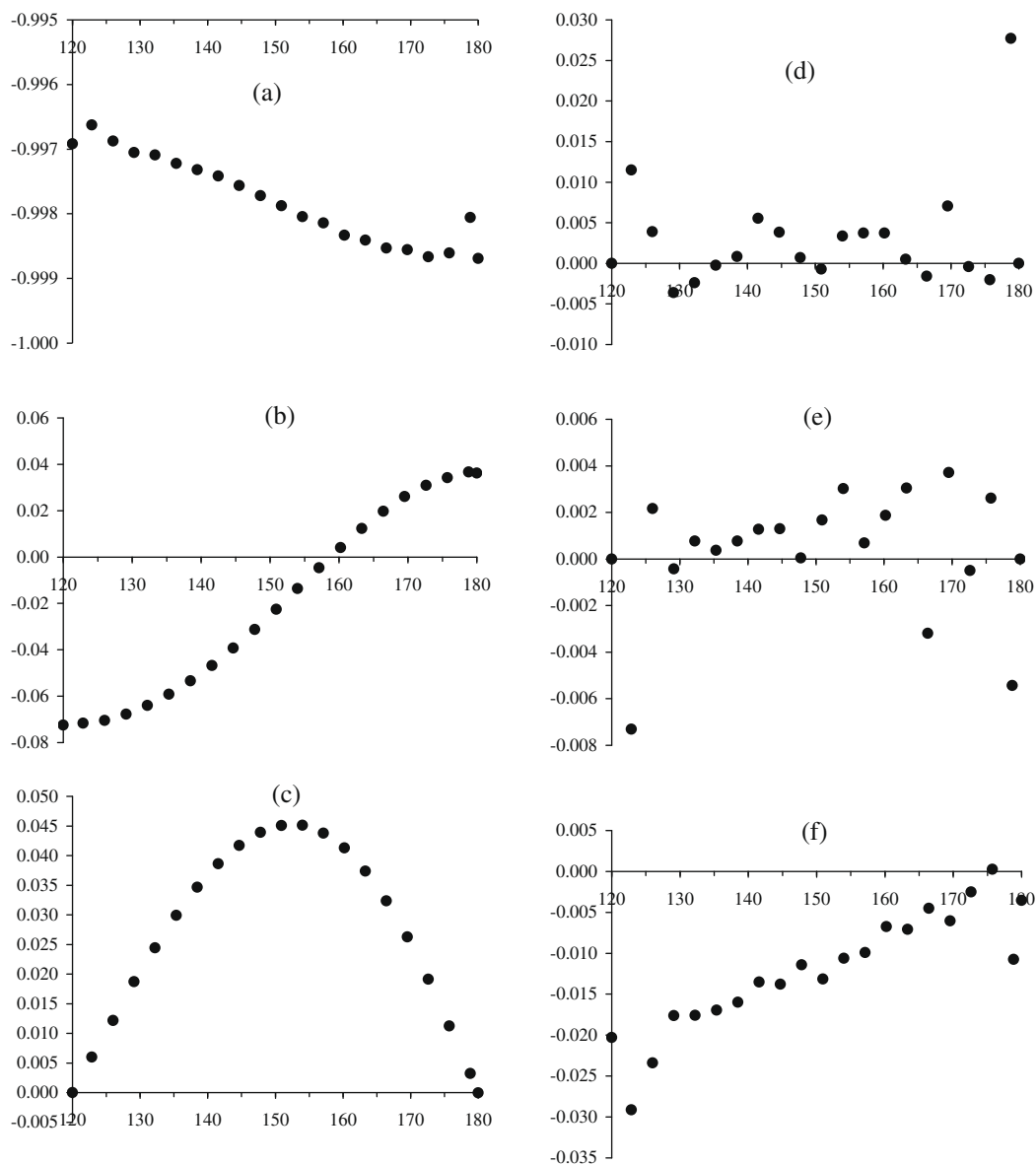
Gaussian supplies vibrational displacement vector components for each projected frequency in non-mass-weighted Cartesian coordinates (standard orientation and five figures after the decimal). As mentioned earlier, various signs in the eigenvector coefficients produced by the diagonalization routine are arbitrary, and they must be adjusted manually at each point along the MEP by performing suitable  $C_{2x}$ ,  $C_{2y}$ ,  $C_{2z}$  and/or  $i$  operations on the displacements to achieve a smooth point-to-point variation of the individual displacement-vector components with  $\gamma$ . This must then be followed by a rotation to the principal axis system at each point, before meaningful Fourier expansions can be attempted.

Table 8 gives a set of Fourier expansion fits for the  $\gamma$ -variation of the vibrational eigenmode atomic displacement vectors in the principal axis system corresponding to projected frequencies for the C–O stretch and the H–O–C bend, as well as the RMS of the fit for each atomic displacement. Similar results were obtained for the O–H stretch, but are not shown here. As illustrated by the two modes in Table 8, most of the 54 atomic displacement vectors for these three modes, which are all “frame vibrations”, can be represented along the MEP by their Fourier expansion coefficients to within a factor of 20 of the expected round-off error of  $3 \times 10^{-6}$  for these five-digit displacements.

On the other hand, the  $\gamma$ -variations of displacement vectors associated with vibrational modes of the methyl-top hydrogens are not well described by short Fourier series. For example, the  $v_4$ ,  $v_{10}$ , and  $v_5$  methyl bending mode displacements require one to two more terms in their Fourier expansions compared to those shown in Table 8. The  $v_2$  and  $v_9$  methyl asymmetric stretch mode displacements cannot be fit at all, which is almost certainly related to the bad fits of the individual projected frequencies  $v_2$  and  $v_9$  described in the previous subsection (see Tables 5–7). Even though it is the  $\gamma$ -variation of vibrational eigenmodes for methyl-top vibrations that are intrinsically the most interesting in this study, we do not attempt to fit these methyl-top-mode displacement vectors here. Before treating these modes, it will be necessary, in our opinion, to carry out a careful investigation of: (i) mixings like those described in connection with the  $v_2/v_9$  vibrational frequencies in the previous subsection, and (ii) the  $(-1)$  factor multiplying certain vibrational wavefunctions after  $2\pi$  rotation of the methyl top, which is associated with half-integral  $n$  values in the Fourier expansions [8] and with the phenomenon of Berry phase [30]. We hope to make an in-depth study of these questions in the future.

## 8. Discussion

The main conclusions of this paper concerning the use of ab initio calculations to aid vibration–torsion–rotation spectroscopic analyses of methanol-like molecules are the following.



**Fig. 3.** Six components of the gradient vector (expressed in symmetrized internal coordinates, as defined by Eqs. (16) and (17)), i.e., six components of the direction of the steepest descent vector (calculated originally in mass-weighted Cartesian coordinates) at each point along the MEP. Panel (a) shows the coefficient of the torsional coordinate  $\tau_{\text{HOCH}}(S_1, A_2)$ . If the MEP were identical to the torsional motion, as defined by the average HOCH dihedral angle, this coefficient would be constant, with magnitude equal to unity. In fact it is nearly unity, but has a small cosine dependence. Note also the noisy behavior for points just after the maximum and just before the minimum of the barrier, presumably associated with numerical difficulties in defining the precise direction of the gradient near stationary points on the potential curve. Panel (b) shows the cosine variation of the next largest coefficient, which corresponds to the (approximate methyl bending) symmetrized internal coordinate  $\beta_{\text{OCH}}(S_3, A_2)$ . Panel (c) shows the sine variation for the (approximate methyl rocking) symmetrized internal coordinate  $\beta_{\text{OCH}}(S_2, A_1)$ . Panels (d)–(f), show components of the steepest-descent vector along the three stretching coordinates  $r_{\text{OH}}(A_1)$ ,  $r_{\text{CH}}(S_1, A_1)$  and  $r_{\text{CH}}(S_3, A_2)$ , which are expected by symmetry to be a sine, sine and cosine curve, respectively, but which are in fact at the noise level of the present quantum chemistry calculations.

(i) The large-amplitude torsion motion can conveniently be defined as motion along the path of steepest descent in mass-weighted Cartesian coordinates, following the recommendations of [12] and the computational options offered by Gaussian [4], but Fourier expansions can be carried out using the average dihedral angle  $\gamma$  [9,10] at points along the steepest-descent path, since, to a good approximation [6],  $\gamma$  is linearly related to distance along the steepest-descent path. (ii) The Gaussian suite of programs [4] is capable of delivering: (a) structural information  $\mathbf{a}_i(\gamma)$ , (b) potential surface information  $V$ ,  $\mathbf{V}\mathbf{V}$ ,  $\mathbf{V}\mathbf{V}\mathbf{V}$ , and (c) projected small-amplitude vibrational frequency information  $\nu_j(\gamma)$  at points  $\gamma$  along the steepest-descent path to levels of self-consistency and absolute accuracy that make this information potentially useful as an aid to high-resolution spectroscopic analyses in energy regions exhibiting

extensive vibration–torsion–rotation interactions. Many of the numerical quantities can be well described by short Fourier expansions in  $\gamma$ . (iii) The only part of the Hessian matrix  $\mathbf{V}\mathbf{V}\mathbf{V}$  that is useful after transforming to vibration–torsion–rotation coordinates is the  $(3N - 7) \times (3N - 7)$  block labeled by the small-amplitude vibrations (because its diagonalized form yields the projected frequencies). (iv) The task of making Fourier expansions of the vibrational displacement vectors is complicated by both small technical problems in treating the Gaussian output and larger theoretical questions.

In view of the good precision and accuracy mentioned above, it is now reasonable to ask exactly how the available ab initio information should be used to help with high-resolution vibration–torsion–rotation analyses. While the detailed answers to this question

**Table 8**

Fourier expansion coefficients of non-mass-weighted displacement-vector components in the principal axis system, in CH<sub>3</sub>OH, as determined for the C–O stretch and the C–O–H bend along the MEP.

	x(H)	y(H)	z(H)	x(O)	y(O)	z(O)	x(C)	y(C)	z(C)
Fourier expansion coefficients for displacements of the H, O, and C frame atoms in Å for the C–O stretch <sup>a,b</sup>									
a <sub>0</sub>	0.318590(2)	0 (fixed)	−0.54091(2)	−0.019461(2)	0 (fixed)	0.24422(2)	−0.043326(6)	0 (fixed)	−0.23965(2)
a <sub>3</sub>	0.016555(3)	0.0522(3)	0.03315(2)	−0.009948(2)	0.00058(2)	0.07419(2)	0.014744(8)	−0.008175(4)	−0.08719(3)
a <sub>6</sub>	−0.000038(3)	0.0013(3)	0.00363(2)	−0.000772(2)	0.00027(2)	0.00334(2)	0.001469(8)	−0.000629(4)	−0.00418(3)
a <sub>9</sub>	−0.000254(3)		−0.00021(2)	0.000049(2)	0.00003(2)	−0.00082(2)	−0.000025(8)	−0.000049(4)	0.00094(3)
a <sub>12</sub>	0.000007(3)		−0.00008(2)	0.000015(2)		−0.00007(2)		0.000008(4)	0.00009(3)
σ <sup>c</sup>	0.000009	0.0010	0.00007	0.00007	0.00007	0.00007	0.000026	0.000012	0.00008
Fourier expansion coefficients for displacements of the H, O, and C frame atoms in Å for the H–O–C bend <sup>a,b</sup>									
a <sub>0</sub>	−0.241305(2)	0 (fixed)	0.755348(3)	0.0819417(7)	0 (fixed)	−0.012614(1)	−0.1213202(9)	0 (fixed)	−0.040696(2)
a <sub>3</sub>	−0.003050(2)	0.0446(2)	0.011427(5)	−0.000315(1)	−0.00047(1)	0.005733(1)	0.004041(1)	−0.008632(2)	−0.010363(2)
a <sub>6</sub>	−0.000406(2)		0.001505(5)	0.000049(1)	0.00030(1)	0.000112(1)	−0.000019(1)	−0.000677(2)	−0.000112(2)
a <sub>9</sub>	−0.000015(2)		0.000104(5)	0.000007(1)		0.000019(1)	−0.000015(1)	−0.000036(2)	−0.000019(2)
σ <sup>c</sup>	0.000006	0.0005	0.000016	0.000003	0.00004	0.000005	0.000004	0.000006	0.000006
	x(S <sub>1</sub> )	y(S <sub>1</sub> )	z(S <sub>1</sub> )	x(S <sub>2</sub> )	y(S <sub>2</sub> )	z(S <sub>2</sub> )	x(S <sub>3</sub> )	y(S <sub>3</sub> )	z(S <sub>3</sub> )
Fourier expansion coefficients for displacements of the three methyl hydrogens in Å for the C–O stretch <sup>d,e</sup>									
a <sub>0</sub>	0.292195(6)	0 (fixed)	−0.27808(2)	0.019809(4)	0 (fixed)	0.54304(2)	0 (fixed)	−0.023152(2)	0 (fixed)
a <sub>3</sub>	−0.019752(9)	0.02072(2)	−0.09956(3)	−0.053011(5)	0.0416(1)	−0.09091(2)	−0.0761(1)	−0.062101(3)	−0.07129(2)
a <sub>6</sub>	−0.003018(9)	0.00113(2)	−0.00398(3)	0.002777(5)	−0.0019(1)	−0.01096(2)	0.0016(1)	−0.000981(3)	−0.00584(2)
a <sub>9</sub>	−0.000123(9)	0.00014(2)	0.00118(3)	0.000197(5)	−0.0002(1)	−0.00008(2)	0.0003(1)	0.000309(3)	−0.00034(2)
a <sub>12</sub>	0.000062(9)	−0.00004(2)	0.00009(3)	−0.000022(5)		0.00020(2)		0.000007(3)	0.00011(2)
σ <sup>c</sup>	0.000029	0.00005	0.00009	0.000017	0.00037	0.00008	0.0004	0.000009	0.00006
Fourier expansion coefficients for displacements of the three methyl hydrogens in Å for the H–O–C bend <sup>d,e</sup>									
a <sub>0</sub>	0.222478(2)	0 (fixed)	−0.040765(3)	0.023800(2)	0 (fixed)	0.511296(5)	0 (fixed)	0.0151994(7)	0 (fixed)
a <sub>3</sub>	−0.023129(3)	0.037876(8)	0.012106(4)	−0.123657(2)	0.10972(6)	0.001986(7)	−0.14233(5)	−0.1272452(9)	−0.03002(1)
a <sub>6</sub>	−0.000091(3)	0.001830(8)	−0.001117(4)	−0.001110(2)	0.00087(6)	−0.000492(7)	−0.00061(5)	−0.0004509(9)	−0.00449(1)
a <sub>9</sub>	0.000048(3)	0.000085(8)	−0.000122(4)	−0.000307(2)	0.00023(6)		−0.00028(5)	−0.0002134(9)	−0.00031(1)
a <sub>12</sub>	0.000006(3)		0.000014(4)	−0.000007(2)				−0.0000165(9)	
σ <sup>c</sup>	0.000009	0.000025	0.000013	0.000008	0.000177	0.000022	0.000164	0.000003	0.00004

<sup>a</sup> Displacements at all points along the IRC, which are printed out with only six decimal places by G03, have been rotated into their principal axis systems. Since the molecule has an *xz* plane of symmetry at the top and bottom of the barrier, the *y*-displacements of all frame atoms for in-plane vibrations are zero at these two points, but not at other points along the MEP.

<sup>b</sup> Fourier expansions for the *x* and *z* displacements have the form  $\sum_n a_{3n} \cos 3n\gamma$ , where *n* is limited to either 2 or 3 in this table. Fourier expansions for the *y*-displacements have the form  $\sum_n a_{3n} \sin 3n\gamma$ , where *n* = 0 is not used in the sum. Numbers in parentheses indicate one standard uncertainty (*k* = 1, type A) [27] from the least-squares fits.

<sup>c</sup> The standard deviations of the fits are given by  $\sigma$ .

<sup>d</sup> The linear combinations *S*<sub>1</sub>, *S*<sub>2</sub> and *S*<sub>3</sub> of the methyl hydrogen displacements used in this table are defined as in Eqs. (16) and (17).

<sup>e</sup> Fourier expansions for the *x* and *z* components of *S*<sub>1</sub> and *S*<sub>2</sub> and for the *y* component of *S*<sub>3</sub> have the form  $\sum_n a_{3n} \cos 3n\gamma$ , where *n* is limited to 3 in this table. Fourier expansions for the *y* component of *S*<sub>1</sub> and *S*<sub>2</sub> and for the *x* and *z* components of *S*<sub>3</sub> have the form  $\sum_n a_{3n} \sin 3n\gamma$ , where *n* = 0 is not used in the sum. Numbers in parentheses indicate one standard uncertainty (*k* = 1, type A) [27] from the least-squares fits.

are not yet known, an important general remark is clear: *ab initio* calculations give adiabatic potential surfaces, in the sense that all interactions arising purely from the potential energy operator have been taken into account. This means that observed spectroscopic complications associated with concepts like perturbations, avoided crossings, intensity borrowings, etc. will have to be explained in terms of interactions arising from the kinetic energy operator, i.e., by interactions arising from operators which differentiate the various adiabatic quantities with respect to the small-amplitude vibrational displacements and the internal rotation angle  $\gamma$ . This is not a particularly appealing way for spectroscopists to have to think, since we intuitively prefer to ignore velocity effects and focus instead on potential energy terms to explain observed spectroscopic complications. In short, it is not clear if a many-atom vibration–torsion–rotation Hamiltonian treatment should proceed from an adiabatic starting point (i.e., proceed directly from the potential surface information provided by Gaussian), or if some artificial adiabatic starting point (where many first derivative terms are small enough to be ignored in any qualitative explanation) should be constructed.

Another important question concerns the use of rectilinear coordinates for the small-amplitude vibrations (upon which all of the work of this paper is based). As discussed in detail elsewhere [31,32], there is reason to worry that rectilinear coordinates are not a good zeroth-order starting point for small-amplitude vibra-

tions along a chemical reaction path. Very preliminary considerations suggest, however, that the difficulties discussed in [31,32] may be less severe along internal rotation MEPs, where the saddle and minimum differ in energy by only a few hundredths of an eV (as is the case for the torsional problem in methanol-like molecules), rather than by a few eV (as is the case for typical chemical reactions).

## Acknowledgments

L.H.X. and R.M.L. thank the Natural Sciences and Engineering Research Council of Canada for financial support of this research program. J. Fisher is grateful for NSERC-USRA (Undergraduate Summer Research Award) support.

## References

- [1] Li-Hong Xu, R.M. Lees, J.T. Hougen, *J. Chem. Phys.* 110 (1999) 3835–3841.
- [2] Li-Hong Xu, *J. Chem. Phys.* 113 (2000) 3980–3989.
- [3] X. Wang, D.S. Perry, *J. Chem. Phys.* 109 (1998) 10795–10805.
- [4] M.J. Frisch, G.W. Trucks, H.B. Schlegel, G.E. Scuseria, M.A. Robb, J.R. Cheeseman, J.A. Montgomery Jr., T. Vreven, K.N. Kudin, J.C. Burant, J.M. Millam, S.S. Iyengar, J. Tomasi, V. Barone, B. Mennucci, M. Cossi, G. Scalmani, N. Rega, G.A. Petersson, H. Nakatsuji, M. Hada, M. Ehara, K. Toyota, R. Fukuda, J. Hasegawa, M. Ishida, T. Nakajima, Y. Honda, O. Kitao, H. Nakai, M. Klene, X. Li, J.E. Knox, H.P. Hratchian, J.B. Cross, V. Bakken, C. Adamo, J. Jaramillo, R. Gomperts, R.E. Stratmann, O. Yazyev, A.J. Austin, R. Cammi, C. Pomelli, J.W. Ochterski, P.Y. Ayala, K.

- Morokuma, G.A. Voth, P. Salvador, J.J. Dannenberg, V.G. Zakrzewski, S. Dapprich, A.D. Daniels, M.C. Strain, O. Farkas, D.K. Malick, A.D. Rabuck, K. Raghavachari, J.B. Foresman, J.V. Ortiz, Q. Cui, A.G. Baboul, S. Clifford, J. Cioslowski, B.B. Stefanov, G. Liu, A. Liashenko, P. Piskorz, I. Komaromi, R.L. Martin, D.J. Fox, T. Keith, M.A. Al-Laham, C.Y. Peng, A. Nanayakkara, M. Challacombe, P.M.W. Gill, B.G. Johnson, W. Chen, M.W. Wong, C. Gonzalez, J.A. Pople, Gaussian 03, Revision B.05.
- [5] Certain commercial products are identified in this paper in order to specify adequately the experimental or theoretical procedures. In no case does such identification imply recommendation or endorsement by the National Institute of Standards and Technology, nor does it imply that the products are necessarily the best available for the purpose.
- [6] Li-Hong Xu, J.T. Hougen, R.M. Lees, M.A. Mekhtiev, *J. Mol. Spectrosc.* 214 (2002) 175–187.
- [7] G. Dellepiane, M. Gussoni, J.T. Hougen, *J. Mol. Spectrosc.* 47 (1973) 515–530.
- [8] J.T. Hougen, *J. Mol. Spectrosc.* 181 (1997) 287–296.
- [9] A.G. Ozkabak, L. Goodman, *J. Chem. Phys.* 96 (1992) 5958–5968.
- [10] V. Szalay, A.G. Császár, M.L. Senent, *J. Chem. Phys.* 117 (2002) 6489–6492.
- [11] W.D. Allen, A. Bodi, V. Szalay, A.G. Császár, *J. Chem. Phys.* 124 (2006) 224310.
- [12] H.B. Schlegel, in: K.P. Lawley (Ed.), *Ab Initio Methods in Quantum Chemistry I*, Wiley, New York, 1987, pp. 249–286.
- [13] D.G. Truhlar, A. Kuppermann, *J. Am. Chem. Soc.* 93 (1971) 1840–1851.
- [14] T.V. Albu, D.G. Truhlar, *J. Mol. Spectrosc.* 219 (2003) 129–131.
- [15] J.C. Corchado, Y.-Y. Chuang, E.L. Coitiño, D.G. Truhlar, GAUSSRATE-version 9.0, University of Minnesota, Minneapolis, 2002.
- [16] J.C. Corchado, Y.-Y. Chuang, P.L. Fast, J. Villá, W.-P. Hu, Y.-P. Liu, G.C. Lynch, K.A. Nguyen, C.F. Jackels, V.S. Melissas, B.J. Lynch, I. Rossi, E.L. Coitiño, A. Fernandez-Ramos, J. Pu, T.V. Albu, R. Steckler, B.C. Garrett, A.D. Isaacson, D.G. Truhlar, POLYRATE-version 9.0, University of Minnesota, Minneapolis, 2002.
- [17] Carlos A. Gonzalez, Private communication.
- [18] Gaussian 98 User's Reference, Version 6.0, pp. 118, 133; Gaussian 03 User's Reference, Version 7.0, pp. 153, 169.
- [19] C.C. Lin, J.D. Swalen, *Rev. Mod. Phys.* 31 (1959) 841–892.
- [20] J.T. Hougen, I. Kleiner, M. Godefroid, *J. Mol. Spectrosc.* 163 (1994) 559–586.
- [21] A. Tachibana, K. Fukui, *Theor. Chim. Acta* 51 (1979) 189–206.
- [22] M.N. Adamov, G.A. Natanson, *Vestn. Lenin. Univ.* (1970) 50–58 (in Russian).
- [23] R.W. Redding, J.T. Hougen, *J. Mol. Spectrosc.* 37 (1971) 366–370.
- [24] Gaussian 03 User's Reference, Version 7.0, p. 127.
- [25] Program GMATPC is Schachtschneider's GMAT modified to work on a PC, as provided by Professor John Bertie, University of Alberta.
- [26] B.P. Winnewisser, J.K.G. Watson, *J. Mol. Spectrosc.* 205 (2001) 227–231.
- [27] Guidelines for Evaluating and Expressing the Uncertainty of NIST Measurement Results, NIST Technical Note 1297, 1994. Available from: <<http://physics.nist.gov/cuu/Uncertainty/index.html>>.
- [28] E.B. Wilson Jr., J.C. Decius, P.C. Cross, *Molecular Vibrations*, McGraw-Hill, New York, 1955.
- [29] T. Shimanouchi, NSRDS-NBS 39, *Tables of Molecular Vibrational Frequencies – Consolidated Volume I*, 1972.
- [30] B. Fehrensen, D. Luckhaus, M. Quack, M. Willeke, T.R. Rizzo, *J. Chem. Phys.* 119 (2003) 5534–5544.
- [31] G.A. Natanson, B.C. Garrett, T.N. Truong, T. Joseph, D.G. Truhlar, *J. Chem. Phys.* 94 (1991) 7875–7892.
- [32] C.F. Jackels, Z. Gu, D.G. Truhlar, *J. Chem. Phys.* 102 (1995) 3188–3201.